# THE MAGNETIC SENSITIVITY OF THE Ba II $D_1$ AND $D_2$ LINES OF THE FRAUNHOFER SPECTRUM

Luca Belluzzi[1,2], Javier Trujillo Bueno[1,3]
and
Egidio Landi Degl'Innocenti[2]

## ABSTRACT

The physical interpretation of the spectral line polarization produced by the joint action of the Hanle and Zeeman effects offers a unique opportunity to obtain empirical information about hidden aspects of solar and stellar magnetism. To this end, it is important to achieve a complete understanding of the sensitivity of the emergent spectral line polarization to the presence of a magnetic field. Here we present a detailed theoretical investigation on the role of resonance scattering and magnetic fields on the polarization signals of the Ba II $D_1$ and $D_2$ lines of the Fraunhofer spectrum, respectively at 4934 Å and 4554 Å. We adopt a three-level model of Ba II, and we take into account the hyperfine structure that is shown by the $^{135}$Ba and $^{137}$Ba isotopes. Despite of their relatively small abundance (18%), the contribution coming from these two isotopes is indeed fundamental for the interpretation of the polarization signals observed in these lines. We consider an optically thin slab model, through which we can investigate in a rigorous way the essential physical mechanisms involved (resonance polarization, Zeeman, Paschen-Back and Hanle effects), avoiding complications due to radiative transfer effects. We assume the slab to be illuminated from below by the photospheric solar continuum radiation field, and we investigate the radiation scattered at 90°, both in the absence and in the presence of magnetic fields, deterministic and microturbulent. We show in particular the existence of a differential magnetic sensitivity of the three-peak $Q/I$ profile that is observed in the $D_2$ line in quiet regions close to the solar limb, which is of great interest for magnetic field diagnostics.

[1]Instituto de Astrofísica de Canarias, Vía Láctea s/n, E-38205 La Laguna, Tenerife, Spain

[2]Università degli Studi di Firenze, Dipartimento di Astronomia e Scienza dello Spazio, Largo Enrico Fermi 2, I-50125 Firenze, Italy

[3]Consejo Superior de Investigaciones Científicas, Spain

*Subject headings:* atomic processes — line: profiles — polarization — scattering — Sun: magnetic fields

## 1. INTRODUCTION

Probably, the most interesting aspect of spectropolarimetry is that it allows us to diagnose magnetic fields in astrophysics. To this end, it is crucial to achieve a complete physical understanding of the magnetic sensitivity of the emergent spectral line radiation given the fact that it can occur through a variety of rather unfamiliar physical mechanisms, not only via the Zeeman effect (e.g., Landi Degl'Innocenti & Landolfi 2004 (hereafter LL04); see also the reviews by Stenflo 2003 and Trujillo Bueno 2003). In this respect, the main aim of this paper is to help decipher the physical mechanisms that control the magnetic sensitivity of the polarization of the D-lines of Ba II, with particular interest in developing a powerful diagnostic tool for mapping the magnetic field of the lower solar chromosphere.

In the atmospheres of the Sun and of other stars there is a fundamental mechanism producing polarization in spectral lines, which has nothing to do with the familiar Zeeman effect. There, where light escapes through the stellar "surface", the atomic system is illuminated anisotropically. The radiative transitions produce population imbalances and quantum coherences between pairs of magnetic sublevels, even among those pertaining to different levels. The mere presence of this so-called atomic level polarization produces spectral line polarization, without the need of a magnetic field. This is usually referred to as resonance line polarization. The important point is that a magnetic field can modify the atomic polarization of the upper and/or lower levels of the spectral line under consideration and the ensuing polarization of the emergent spectral line radiation. Interestingly, the possible presence of crossings and repulsions among magnetic sublevels of fine-structure and/or hyperfine-structure multiplets can enhance dramatically the magnetic sensitivity of the emergent spectral line polarization. A remarkable example is the enhancement of the line-core scattering polarization of the $D_2$ line of Na I by a vertical magnetic field, which is due to interferences between particular hyperfine structure (HFS) magnetic sublevels of the $^2P_{3/2}$ upper level (Trujillo Bueno et al. 2002). It is of interest to note that this theoretical prediction was observationally confirmed by Stenflo et al. (2002) via filter polarimetry of the solar atmosphere.

In contrast with the case of sodium, which has one single isotope with nuclear spin I=3/2, barium has five (even) isotopes with I=0 (with an overall abundance of 82.18%) and two (odd) isotopes with I=3/2 (with an abundance of 17.82%). Moreover, the HFS split-

ting of the odd isotopes of barium is about a factor five larger than for the case of sodium. Obviously, the emergent fractional linear polarization (i.e., the $Q/I$ profile, where $I$ and $Q$ are two of the Stokes parameters) has contributions from all the barium isotopes. In fact, as pointed out by Stenflo (1997), the $Q/I$ pattern of the Ba II $D_2$ line that Stenflo & Keller (1997) observed in very quiet regions close to the solar limb shows a three-peak structure, with a prominent central $Q/I$ peak due to the even isotopes (which are devoid of HFS) and two less significant peaks in the red and blue wings caused by the contributions from the odd isotopes (which have HFS). Therefore, we think that for the $D_2$ line of Ba II we should also have enhancement of scattering polarization by a vertical field, but only around such wing wavelengths because the required interferences occur only between the magnetic sublevels of the $^2P_{3/2}$ upper level of the barium isotopes endowed of HFS. Actually, the scientific motivation that led us to undertake the theoretical investigation presented here was to develop a novel plasma diagnostic tool based on the idea that such isotopes of barium must have a different behavior in the presence of a magnetic field, with respect to those devoid of HFS.

While the physical origin of the observed $Q/I$ profile of the Ba II $D_2$ line seems to be clear, nobody has yet been able to model the $Q/I$ profiles of the Ba II $D_1$ line that Stenflo et al. (1998) observed in two different regions close to the solar limb. Interestingly, while the $Q/I$ profile shown in Fig. 1 of Stenflo et al. (1998) might perhaps be the result of the interaction of the $D_1$ line with the continuum (see the bottom panel to the right-hand-side), the symmetric $Q/I$ profile shown in the panel just above the previous one is very similar to the enigmatic $Q/I$ profile of the Na I $D_1$ line (see also Fig. 3 in Stenflo et al. 2000). Although the main scientific target of our paper is to understand the magnetic sensitivity of the above-mentioned Ba II $D_2$ line, we present also some results of our $Q/I$ calculations for the $D_1$ line with the aim of helping to clarify its physical origin.

The outline of this paper is the following. The formulation of the problem is presented in Section 2, where we establish our modeling assumptions, we briefly discuss the relevant equations, and we describe the atomic model, showing the behaviour of the magnetic sublevels of the odd barium isotopes in the presence of an increasing magnetic field. The magnetic sensitivity of the atomic polarization of the lower and upper levels of the Ba II D-lines is discussed in Section 3, pointing out the similarities with the behavior of the Na I levels. Section 4 focuses on the emergent spectral line polarization in the absence and in the presence of a magnetic field, with emphasis on the $D_2$ line of Ba II, but showing also some interesting results for the $D_1$ line. Finally, Section 5 summarizes our main conclusions with an outlook to future research. The three appendices give detailed information that may help the reader to understand better the complexity of the problem we are investigating.

## 2. FORMULATION OF THE PROBLEM

We consider an optically thin slab of Ba II ions illuminated from below by the photospheric solar continuum radiation field (see Fig. 1). The slab is assumed to be located 1000 km above the $\tau_{5000}=1$ photospheric level, the approximate height at which, according to semi-empirical models of the solar atmosphere, the line-core optical depth of the $D_2$ line is unity along a line-of-sight specified by $\mu\equiv\cos\theta=0.1$, with $\theta$ the heliocentric angle.

In the following subsections we summarize the basic equations derived within the framework of the quantum theory of spectral line polarization that will be used in this work (§ 2.1), we describe the atomic model that we have adopted to describe the Ba II ion (§ 2.2), and finally we show how the main properties of the continuum photospheric radiation field incident on the slab have been calculated (§ 2.3).

### 2.1. *The Basic Equations*

We describe the excitation state of the Ba II levels using the density matrix formalism, a robust theoretical framework very suitable to treat the atomic polarization (population imbalances and quantum interferences, or coherences, among the magnetic sublevels) that anisotropic pumping processes induce in an atomic system. Referring to one of the isotopes of barium (see § 2.2) that shows HFS, we indicate with $I$ its nuclear spin quantum number. In the absence of magnetic fields, using Dirac's notation, the energy eigenvectors can be written in the form $|\alpha\, J\, I\, F\, f>$, where $\alpha$ represents a set of inner quantum numbers (specifying the electronic configuration and, if the atomic system is described in the L-S coupling scheme, the total electronic orbital and spin angular momenta), $J$ is the total electronic angular momentum quantum number, $F$ is the total angular momentum quantum number (electronic plus nuclear: $\boldsymbol{F}=\boldsymbol{J}+\boldsymbol{I}$), and $f$ is its projection along the quantization axis. In principle, to have a suitable description of atomic polarization, one has to take into account all the coherences of the form

$$<\alpha\, J\, I\, F\, f\,|\,\hat{\rho}\,|\,\alpha\, J'\, I\, F'\, f'>\ , \tag{1}$$

where $\hat{\rho}$ is the density matrix operator. The approximation that is used in this paper consists in restricting the description of the atomic system to the $J$-diagonal density matrix elements

$$<\alpha\, J\, I\, F\, f\,|\,\hat{\rho}\,|\,\alpha\, J\, I\, F'\, f'>\ , \tag{2}$$

or, in other words, in neglecting coherences between different $J$-levels. The resulting model-atom is referred to as the "multi-level atom with hyperfine structure" according to LL04. The approximation appears to be fully justified for the investigation of the Ba II D-lines given the large frequency separation between the levels $6p\ ^2P_{1/2}$ and $6p\ ^2P_{3/2}$ (see § 2.2), and

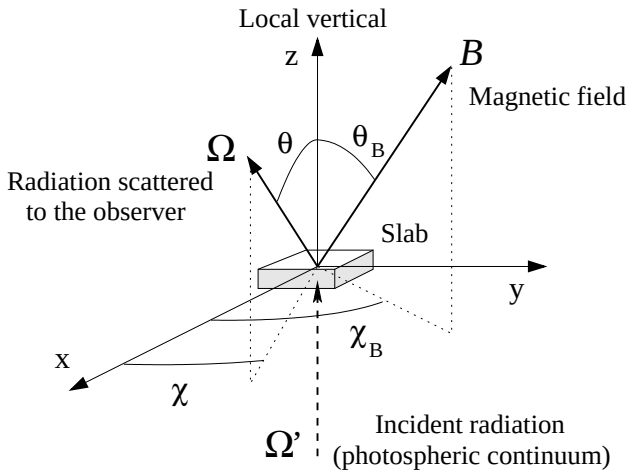


Fig. 1.— Geometry of the problem under investigation.

given the relatively low abundance of barium in the solar atmosphere[1].

In the presence of a magnetic field, according to the general approach of the Paschen-Back effect theory, the energy eigenvalues and eigenvectors have to be found by diagonalization of the total Hamiltonian (unperturbed atomic Hamiltonian plus magnetic Hamiltonian) on each $J$-level subspace. Taking the quantization axis along the magnetic field direction, it can be demonstrated that the total Hamiltonian commutes with the projection along the quantization axis of the total angular momentum operator ($f$ is a good quantum number), while, in general, it does not commute with the total angular momentum operator. The eigenvectors of the total Hamiltonian can be expressed in the form (e.g. LL04)

$$|\alpha\, J\, I\, i\, f >= \sum_F C_F^i\,(\alpha\, J\, I,\, f\,)\,|\alpha\, J\, I\, F\, f > \ , \tag{3}$$

where the index $i$ labels the energy eigenstates belonging to the subspace corresponding to assigned values of the quantum numbers $\alpha$, $J$, $I$ and $f$, and where the coefficients $C_F^i$ can be chosen to be real. In the energy eigenvectors representation the atomic system will therefore be described by means of the matrix elements

$$< \alpha\, J\, I\, i\, f\,|\,\hat{\rho}\,|\alpha\, J\, I\, i'\, f' >\equiv \rho_{\alpha\, J\, I}(i\, f,\, i'\, f') \ . \tag{4}$$

If the magnetic field is so weak that the magnetic energy is much smaller than the energy intervals between the HFS $F$-levels, we are in the so-called *Zeeman effect regime* (of HFS),

[1]Note that this approximation is not justified for the D-lines of Na I and for the H and K lines of Ca II, given the larger abundance of these ions.

where the energy eigenvectors are still of the form $|\alpha\, J\, I\, F\, f>$ ($C_F^i \simeq \delta_{Fi}$), and the splitting between the HFS magnetic sublevels is linear with the magnetic field strength. For stronger magnetic fields it is necessary to apply the Paschen-Back effect theory, and one enters the so-called *incomplete Paschen-Back effect regime*. In this regime the energy eigenvectors have the general form of equation (3) (the magnetic field produces a $F$-mixing of the various HFS levels originating from a particular $J$-level) and, as we will show in detail for the case of Ba II in § 2.2, the splitting among the various HFS magnetic sublevels is no longer linear with the magnetic field. Several crossings among HFS magnetic sublevels with different $f$ quantum number take place in this regime, as well as a repulsion among the magnetic sublevels with the same $f$ quantum number. This behaviour of the magnetic sublevels has important consequences on the atomic polarization, as pointed out by Bommier (1980) and described in detail in LL04, and produce interesting effects, sometimes referred to as *level crossing effect* and *anti-level-crossing effect*, on the polarization signals produced by resonance scattering (e.g., Trujillo Bueno et al. 2002). In § 4.3 we will show their effect on the linear polarization of the Ba II $D_2$ line. If the magnetic field strength is further increased the so-called *complete Paschen-Back effect regime* is reached. In this regime the energy eigenvectors are of the form $|\alpha\, J\, I\, M_J\, M_I>$, and the splitting among the HFS magnetic sublevels is again linear with the magnetic field strength: the atom behaves in this regime as if it were devoid of HFS. Going from the Zeeman effect regime to the complete Paschen-Back effect regime, the magnetic field produces therefore an energy eigenvectors basis transformation.

In the following we will work in the spherical statistical tensor representation. The conversion of the density matrix elements of equation (4) into this representation is given by the relation (cf. LL04)

$$\rho_{\alpha\, J\, I}(i\, f,\, i'\, f') = \sum_{F F'} C_F^i(\alpha\, J\, I,\, f)\, C_{F'}^{i'}(\alpha\, J\, I,\, f')\, \rho_{\alpha\, J\, I}(F\, f,\, F'\, f') =$$

$$= \sum_{F F'} C_F^i(\alpha\, J\, I,\, f)\, C_{F'}^{i'}(\alpha\, J\, I,\, f') \sum_{K Q} (-1)^{F-f} \sqrt{2K+1} \begin{pmatrix} F & F' & K \\ f & -f' & -Q \end{pmatrix} {}^{\alpha\, J\, I}\rho_Q^K(F, F') \quad . \quad (5)$$

The Statistical Equilibrium Equations (SEEs) and the radiative transfer coefficients for a multi-level atom with HFS, in the spherical statistical tensor representation, written taking the quantization axis directed along the magnetic field, can be found in § 7.9 of LL04. Here we write only the expression for the emission coefficient in the transition between the upper level $(\alpha_u, J_u)$ and the lower level $(\alpha_\ell, J_\ell)$

$$\varepsilon_j(\nu, \mathbf{\Omega}) = \frac{2h\nu^3}{c^2} \frac{h\nu}{4\pi} \mathcal{N}(2J_u+1) B(\alpha_u J_u I \rightarrow \alpha_\ell J_\ell I)$$
$$\times \sum_{K Q K_u Q_u} \sqrt{3(2K+1)(2K_u+1)} \sum_{i_u F_u F'_u F''_u i_\ell F_\ell F'_\ell} \sum_{f_u f'_u f_\ell q q'} (-1)^{1+F'_u-f_u+q'}$$

$$\times C^{i_\ell}_{F_\ell}(\alpha_\ell J_\ell I, f_\ell)\, C^{i_\ell}_{F'_\ell}(\alpha_\ell J_\ell I, f_\ell)\, C^{i_u}_{F_u}(\alpha_u J_u I, f_u)\, C^{i_u}_{F''_u}(\alpha_u J_u I, f_u)$$
$$\times\sqrt{(2F_\ell+1)(2F'_\ell+1)(2F_u+1)(2F'_u+1)}$$
$$\times\begin{pmatrix} F_u & F_\ell & 1 \\ -f_u & f_\ell & -q \end{pmatrix}\begin{pmatrix} F'_u & F'_\ell & 1 \\ -f'_u & f_\ell & -q' \end{pmatrix}\begin{pmatrix} 1 & 1 & K \\ q & -q' & -Q \end{pmatrix}$$
$$\times\begin{pmatrix} F'_u & F''_u & K_u \\ f'_u & -f_u & -Q_u \end{pmatrix}\begin{Bmatrix} J_u & J_\ell & 1 \\ F_\ell & F_u & I \end{Bmatrix}\begin{Bmatrix} J_u & J_\ell & 1 \\ F'_\ell & F'_u & I \end{Bmatrix}$$
$$\times\mathrm{Re}\Big[\mathcal{T}^K_Q(j,\mathbf{\Omega})\,{}^{\alpha_u J_u I}\rho^{K_u}_{Q_u}(F'_u,F''_u)\,\Phi(\nu_{\alpha_u J_u I i_u f_u,\alpha_\ell J_\ell I i_\ell f_\ell}-\nu)\Big]\,, \qquad (6)$$

where $j=0,1,2,3$, standing respectively for the Stokes parameters $I,Q,U$ and $V$, $\mathcal{N}$ is the number density of atoms, $B(\alpha_u J_u I \rightarrow \alpha_\ell J_\ell I)$ is the Einstein coefficient for stimulated emission, $\mathcal{T}^K_Q(j,\mathbf{\Omega})$ is a geometrical tensor (cf. LL04), and $\Phi$ the profile of the line.

It is important to note that the previous equations are valid under the *flat-spectrum approximation*. For a multi-level atom with HFS this approximation requires that the incident radiation field should be flat (i.e. independent of frequency) across a spectral interval $\Delta\nu$ larger than the frequency intervals among the HFS levels (possibly split by the magnetic field), and larger than the inverse lifetimes of the same levels. This is a good approximation for the $D_1$ and $D_2$ lines of Ba II if we restrict to magnetic fields smaller or of the order of 1 kG.

### 2.2. *The Atomic Model*

We adopt a three-level model of Ba II consisting in the ground level ($6s\ ^2S_{1/2}$), the upper level of the $D_1$ line ($6p\ ^2P_{1/2}$) and the upper level of the $D_2$ line ($6p\ ^2P_{3/2}$). There are seven stable isotopes of barium, whose mass numbers and relative abundances are listed in Table 1. In this work we take into account the contributions coming from all the seven isotopes.

The mass and volume differences between the nuclei of the various isotopes involve small but appreciable differences on the energies of the fine structure levels of different isotopes (isotopic effect). We use the values of the isotopic shifts in the $D_1$ and $D_2$ lines listed in Table 1 to correct the energies of the $^2P_{1/2}$ and $^2P_{3/2}$ levels of the variuos isotopes. For the reference isotope (138) we use the energy values given by Moore (1958).

Isotopes with even mass number have nuclear spin $I=0$, while those with odd mass number (135 and 137) have nuclear spin $I=3/2$. The odd isotopes show therefore HFS due to nuclear spin. Introducing the total angular momentum, characterized by the quantum number $F$, we observe (see Fig. 2) that the levels $^2S_{1/2}$ and $^2P_{1/2}$ split into two HFS levels ($F=1,2$), while the level $^2P_{3/2}$ splits into four HFS levels ($F=0,1,2,3$). It is possible to demonstrate that the HFS Hamiltonian can be expressed as an infinite series of electric and

| Isotope | Abund. (%)[a] | $I$ | Isotope Shifts (MHz)[1] | | HFS Constants (MHz)[2] | | | |
|---|---|---|---|---|---|---|---|---|
| | | | $D_1$ | $D_2$ | $^2S_{1/2}$ | $^2P_{1/2}$ | $^2P_{3/2}$ | |
| | | | | | $\mathcal{A}$ | $\mathcal{A}$ | $\mathcal{A}$ | $\mathcal{B}$ |
| $^{130}$Ba | 0.106 | 0 | 355.3[b] | 372.3[b] | | | | |
| $^{132}$Ba | 0.101 | 0 | 278.9[b] | 294.9[b] | | | | |
| $^{134}$Ba | 2.417 | 0 | 222.6[c] | 234.6[c] | | | | |
| $^{135}$Ba | 6.592 | 3/2 | 348.6[b] | 360.7[b] | 3591.67[d] | 664.6[e] | 113.0[e] | 59.0[e] |
| $^{136}$Ba | 7.854 | 0 | 179.4[b] | 186.9[b] | | | | |
| $^{137}$Ba | 11.232 | 3/2 | 271.1[b] | 279.0[b] | 4018.87[d] | 743.7[e] | 127.2[e] | 92.5[e] |
| $^{138}$Ba | 71.698 | 0 | reference isot. | | | | | |

[1]A positive I.S. means that the line is shifted to higher frequencies with respect to the reference isotope.
[2]The HFS constant $\mathcal{B}$ is defined according to the convention of the American literature.
[a]NIST on-line database; [b]Wendt et al. (1984); [c]Wendt et al. (1988); [d]Becker et al. (1981); [e]Villemoes et al. (1993).

Table 1: Isotopes considered in this work.

magnetic multipoles (e.g. Kopfermann 1958). To calculate the energies of the various HFS levels we consider the first two terms of the series (magnetic dipole and electric quadrupole terms), and we use the HFS constants listed in Table 1. This investigation will clearly show the importance of the HFS effects for a correct modeling of the polarization produced by scattering processes in a stellar atmosphere.

The Landé factors have been calculated theoretically, assuming L-S coupling for the Ba II ion. The values obtained differ by less than 1.3% from the experimental ones (Moore 1958), reported in Figure 2. This can be considered as a proof that the L-S coupling is quite a good approximation for the Ba II ion.

The energies of the HFS magnetic sublevels of the isotope 137, as functions of the magnetic field strength, are shown in Figure 2. We can see that in the range between 0 and 1000 G the splitting of the various magnetic sublevels originating from the ground level $^2S_{1/2}$ is linear with the magnetic field strength (Zeeman effect regime). A similar behaviour is shown by the magnetic sublevels originating from the level $^2P_{1/2}$ for magnetic fields smaller than about 600 G. For stronger magnetic fields the linearity of the splitting appears to be slowly lost, which indicates that the incomplete Paschen-Back effect regime is reached. The splitting observed among the magnetic sublevels originating from the level $^2P_{3/2}$ shows instead that a complete transition from the Zeeman effect regime to the complete Paschen-Back effect regime takes place for magnetic fields ranging from 0 to 1000 G. As described in § 2.1, in the intermediate incomplete Paschen-Back effect regime several level crossings among HFS magnetic sublevels can be observed, as well as a repulsion among the sublevels with the same $f$ quantum number.

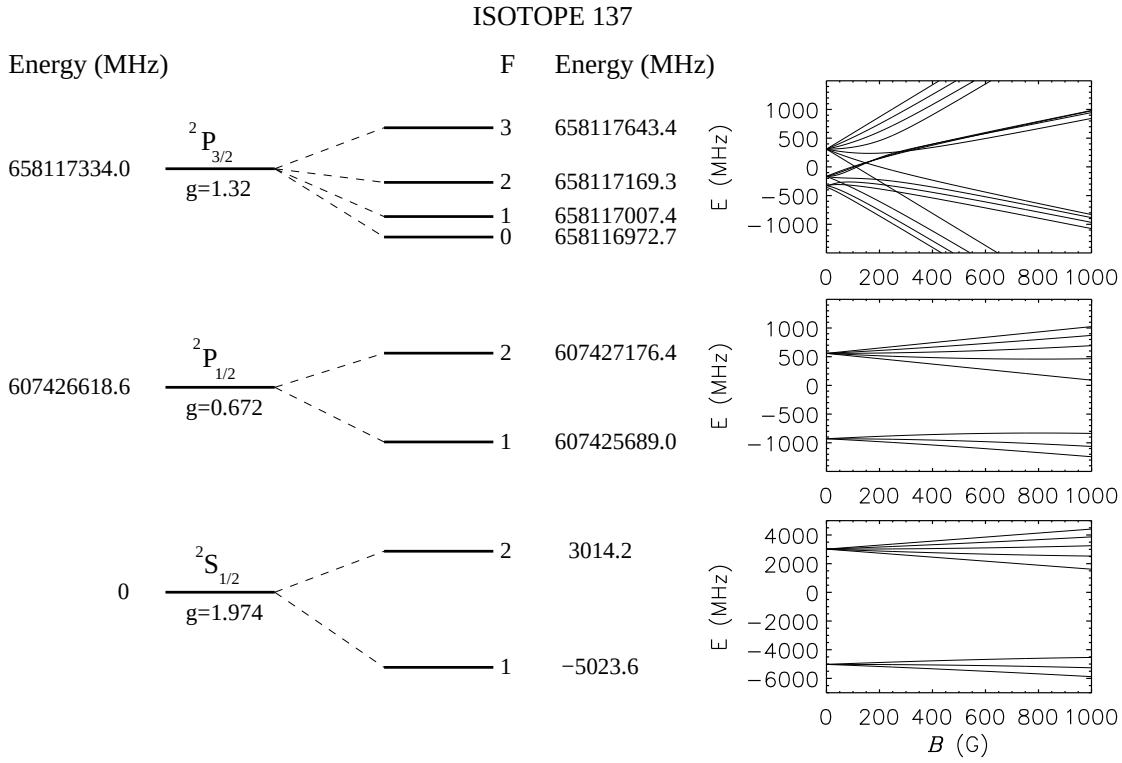


Fig. 2.— Energies, corrected for the isotopic effect, of the fine-structure and HFS levels of the isotope $^{137}$Ba II. The right panels show the energies of the HFS magnetic sublevels as functions of the magnetic field strength (in each panel the zero of the energy scale is chosen at the energy of the corresponding fine structure $J$-level).

### 2.3. *The Incident Radiation Field*

As already stated in § 2, we consider an optically thin plane-parallel slab, composed of Ba II ions, located at approximately 1000 km above the $\tau_{5000}=1$ photospheric level, and we assume that the slab is illuminated from below (hence, anisotropically) by the photospheric continuum radiation. Under these hypothesis the atomic polarization can be calculated solving directly the SEEs for the given continuum radiation field coming from the photosphere.

Let us take a reference system with the $z$ axis directed along the local vertical, and let us describe the continuum radiation field incident on the slab by means of the tensor

$$J^K_Q(\nu) = \int \frac{\mathrm{d}\Omega}{4\pi} \sum_{i=0}^{3} \mathcal{T}^K_Q(i,\mathbf{\Omega}) S_i(\nu,\mathbf{\Omega}) \ , \tag{7}$$

| Line | $\lambda$ (Å) | $A\,(s^{-1})$ | $\bar{n}_\nu$ | $w_\nu$ |
|---|---|---|---|---|
| $D_1$ | 4934.09 | $0.955\times10^{8}$ | $0.323\times10^{-2}$ | 0.159 |
| $D_2$ | 4554.03 | $1.17\times10^{8}$ | $0.225\times10^{-2}$ | 0.176 |

Table 2: Wavelength (in air), and Einstein coefficient of the transitions considered; mean number of photons and anisotropy factor of the photospheric continuum at the wavelength of the transitions, 1000 km above the $\tau_{5000} = 1$ level.

where $S_i = I, Q, U, V$. Assuming that the incident radiation field is unpolarized and has cylindrical symmetry around the local vertical, it is easy to verify that the only non vanishing components are

$$J^0_0(\nu)=\oint \frac{\mathrm{d}\Omega}{4\pi} I(\nu,\mu) \quad \text{and} \quad J^2_0(\nu)=\oint \frac{\mathrm{d}\Omega}{4\pi}\Big(\frac{1}{2\sqrt{2}}(3\mu^2-1)I(\nu,\mu)\Big) \ . \tag{8}$$

Note that $J^0_0$ is just the mean intensity of the incident radiation (averaged over all directions), while $J^2_0$ gives a measure of the anisotropy of the radiation field[2]. Instead of $J^0_0$ and $J^2_0$, we can use the quantities $\bar{n}(\nu)$, the mean number of photons, and $w_\nu$, the so called anisotropy factor. The new quantities are related to the previous radiation field tensor components through the relations

$$\bar{n}(\nu)=\frac{c^2}{2h\nu^3}J^0_0(\nu) \quad \text{and} \quad w_\nu=\sqrt{2}\,\frac{J^2_0(\nu)}{J^0_0(\nu)} \ . \tag{9}$$

To calculate the values of $\bar{n}(\nu)$ and $w_\nu$ of the photospheric continuum at the height of 1000 km above the visible solar "surface", at the frequencies of the $D_1$ and $D_2$ lines of Ba II, we follow § 12.3 of LL04. The values of the specific intensity of the radiation coming from the solar disk center and of the limb-darkening coefficients are taken from Pierce (2000). The values obtained for $\bar{n}_\nu$ and $w_\nu$ are listed in Table 2. At this point the SEEs can be solved numerically. Their expression becomes simpler if we rewrite them in the reference system with the quantization axis directed along the local vertical direction, as in this case only two components of the radiation field tensor are non zero ($J^0_0$ and $J^2_0$). It can be demonstrated that all the radiative rates are invariant under a rotation of the reference system so that only the magnetic kernel has to be modified with respect to the expression given in equation (7.66) of LL04.

[2]In particular $J^2_0$ quantifies the unbalance between vertical and horizontal illuminations.

## 3. THE POLARIZATION OF THE ATOMIC LEVELS

We solve numerically the SEEs (which implies, for each isotope with HFS of our model atom, the solution of a linear system of 384 equations in the unknowns $\rho^K_Q(F,F')$) for magnetic field strengths between 0 and 1000 G, and for various inclinations of the magnetic field with respect to the local vertical. We recall that the $\rho^0_0(F,F)$ elements quantify the populations of the various $F$-levels, the $\rho^2_Q$ elements (*alignment* components) contribute to the linear polarization of the scattered radiation, while the $\rho^1_Q$ elements (*orientation* components) contribute to the circular polarization of the scattered radiation. As shown in LL04, an anisotropic, unpolarized, flat spectrum radiation field generally induces only alignment in the atomic system, while orientation can be originated by the so called alignment-to-orientation conversion mechanism. Note that all the levels of the isotopes 135 and 137, because of the HFS, can carry alignment while, for all the other isotopes, only the level $^2P_{3/2}$, the upper level of the $D_2$ line, can carry it.

Let us consider isotope 137. In complete analogy with the case of Na I, having a single isotope with $I=3/2$ (see Trujillo Bueno et al. 2002 and Casini et al. 2002, and the discussion therein), only the level $^2P_{3/2}$ is polarized directly via the anisotropic illumination. The ground level becomes polarized because of a transfer of polarization via spontaneous emission in the $D_2$ line, while the level $^2P_{1/2}$ becomes polarized via radiative absorption (*repopulation pumping*) in the $D_1$ line. This explains the fact that the upper and lower levels of the $D_1$ line are equally sensitive to the magnetic field strength, independently of its inclination (see Fig. 3).

It is well known that a magnetic field is able to modify the atomic polarization, and therefore the polarization of the scattered radiation (Hanle effect[3]). The behaviour of the various spherical statistical tensors, written in the local vertical reference system, as functions of the magnetic field inclination and strength, is qualitatively equal to the case of Na I, investigated by Trujillo Bueno et al. (2002). We point out that the first decrease of the atomic polarization of the $D_1$ levels, which takes place only for inclined fields (see Fig. 3), is

[3]In this work by Hanle effect we mean any modification of the atomic polarization which is due to the action of a magnetic field. Note, however, that in the literature it is often meant by Hanle effect only the relaxation of coherences (defined in the magnetic field reference system) having $Q \neq 0$. Within this second meaning, it is often stated that there is no Hanle effect in the presence of a vertical magnetic field. Note that according to our definition this statement is true only if we are dealing with an isolated level (i.e. if we neglect the quantum interferences among the magnetic sublevels originating from different hyperfine (or fine) structure levels). We prefer to adopt the former more general definition because, as we are dealing with a quite complex atomic system with HFS, and as we are investigating the role of magnetic fields with complex configurations (random-azimuth and microturbulent), it becomes quite difficult to understand which effects due to the magnetic field can be considered as 'Hanle effect' according to the latter definition.

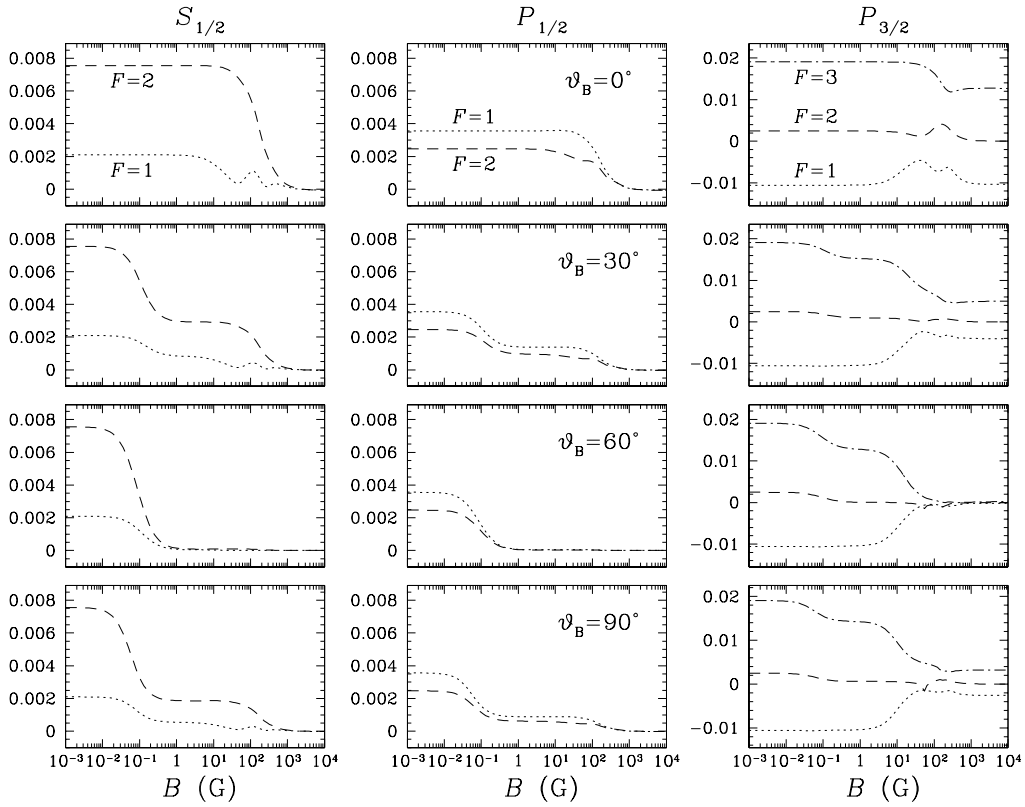


Fig. 3.— Fractional atomic alignment, $\sigma_0^2 = \rho_0^2(F,F)/\rho_0^0(F,F)$, of the various HFS levels of the isotope 137, calculated in the local vertical reference system, as functions of the magnetic field vector, for various inclination angles. Top row $\theta_B = 0°$, middle rows $\theta_B = 30°$ and $\theta_B = 60°$, bottom row $\theta_B = 90°$. The angle $\theta_B$ is defined in Figure 1.

due to the so called lower-level Hanle effect[4]. As can be demonstrated (see LL04 for details), the spherical statistical tensors $\rho^K_Q(F,F)$ (that describe population imbalances and quantum interferences among magnetic sublevels originating from the same $F$-level, and that mainly affect the polarization of the scattered radiation at the line center) are significantly modified by a magnetic field when the Zeeman splitting is of the same order of magnitude as the inverse lifetime of the level. That is, as a rough estimation, when the magnetic field ranges between (see LL04)

$$0.1\, B_{\rm c} \leq B \leq 10\, B_{\rm c} \quad , \tag{10}$$

[4]This definition has been formulated within the latter definition of the Hanle effect given in the footnote 3.

with

$$B_{\rm c} \approx \frac{1.137 \times 10^{-7}}{t_{\rm life}\, g_{\rm L}} \quad , \tag{11}$$

where $t_{\rm life}$ (in seconds) is the radiative lifetime of the lower or upper level of the line transition under consideration, $g_{\rm L}$ is its Landé factor and $B_{\rm c}$ is the critical magnetic field intensity in G[5]. Since the relevant atomic level here is the ground level, it is important to note that its radiative lifetime is $t_{\rm life} \approx 1/(B_{\ell u}\, J^0_0)$. As seen in Figure 3 this first decrease takes place for magnetic fields of the order of $10^{-1}$G, consistently with our simplifying assumption that the pumping radiation field is the continuum radiation tabulated by Pierce (2000). If, on the contrary, one takes into account the line profile (resulting in a smaller value of $J^0_0$) the decrease will take place for smaller magnetic fields (cf. the Na I results of Trujillo Bueno et al. 2002). Note that this decrease of the atomic polarization in the ground level has a feedback even on the $D_2$ upper level. Concerning the second sudden decrease of the atomic polarization of the $D_1$ levels, for $B$ larger than 100 G, we recall that this is due to the inhibition of the repopulation pumping mechanism discussed by Trujillo Bueno et al. (2002) and by Casini et al. (2002), which sets in when the electronic and nuclear angular momenta, $J$ and $I$, of the $^2P_{3/2}$ level are decoupled, (i.e. when this level, the only one that can carry alignment even in the absence of HFS, enters the complete Paschen-Back effect regime). Note that for the case of sodium this sudden decrease occurs for $B$ larger than 10 G simply because the complete Paschen-Back effect regime is reached for weaker magnetic fields in sodium than in barium.

As expected, because of the symmetry of the problem, for a vertical magnetic field only the components with $Q=0$ are non zero. For different orientations of the magnetic field we have in general contributions coming from all the density matrix elements; in particular it is possible to demonstrate that the components with $Q=0$ are independent of the magnetic field azimuth, the components with $Q=1$ change sign under an azimuth rotation of 180°, the components with $Q=2$ change sign under an azimuth rotation of 90°, and so on.

The expressions of the emission coefficients (eq. 6), as well as the expressions of all the other radiative transfer coefficients given in LL04 hold in the magnetic reference system. Therefore we have to transform the spherical statistical tensors, obtained solving the SEEs written in the local vertical reference system, into the magnetic field reference system. Indicating with $[\rho^K_Q(F,F')]_B$ the spherical statistical tensor components in the magnetic field reference system, and with $[\rho^K_Q(F,F')]_V$ the spherical statistical tensor components in the local vertical reference system, we have

$$[\rho^K_Q(F,F')]_B = \sum_{Q'} [\rho^K_{Q'}(F,F')]_V\, D^K_{Q'Q}(R)^* \quad , \tag{12}$$

[5]The previous expression of $B_{\rm c}$ is exact only for an isolated level (see footnote3).

where $D^K_{Q'Q}(R)$ is the rotation matrix calculated for the rotation $R$ which carries the vertical reference system into the magnetic reference system (referring to Fig. 1, we have $R = (\chi_B, \theta_B, 0)$), and where the apex " $*$ " indicates the complex conjugate. We observe that after the rotation, because of the symmetry of the problem, the spherical statistical tensors in the magnetic reference system do not depend on the azimuth but only on the inclination of the magnetic field with respect to the local vertical reference system.

## 4. THE POLARIZATION OF THE EMERGENT SPECTRAL LINE RADIATION

For the case of a tangential observation in a plane-parallel atmosphere, it can be shown that, under the approximation of a weakly polarizing atmosphere ($\varepsilon_I \gg \varepsilon_Q, \varepsilon_U, \varepsilon_V$; $\eta_I \gg \eta_Q, \eta_U, \eta_V$), the emergent fractional polarization is given by (e.g., Trujillo Bueno 2003)

$$\frac{X(\nu, \mathbf{\Omega})}{I(\nu, \mathbf{\Omega})} \approx \frac{\varepsilon_X(\nu, \mathbf{\Omega})}{\varepsilon_I(\nu, \mathbf{\Omega})} - \frac{\eta_X(\nu, \mathbf{\Omega})}{\eta_I(\nu, \mathbf{\Omega})} \qquad \text{with } X = Q, U, V \ . \tag{13}$$

We point out that the first term of equation (13) is the contribution to the emergent fractional polarization due to selective emission processes, while the second one is caused by dichroism (selective absorption of polarization components). As shown in Figure 3, for the $D_2$ line the contribution due to dichroism is much smaller than that due to selective emission. For this reason, from now on we will describe the polarization properties of the radiation emergent from the slab using the relation

$$\frac{X(\nu, \mathbf{\Omega})}{I(\nu, \mathbf{\Omega})} = \frac{\varepsilon_X(\nu, \mathbf{\Omega})}{\varepsilon_I(\nu, \mathbf{\Omega})} \ . \tag{14}$$

We recall that the polarization properties of the emergent radiation will always be described assuming the reference direction for positive $Q$ parallel to the slab.

It is important to remember that the expressions for the emission and absorption coefficients given in LL04 take into account only the line processes. For this reason, in order to be able to reproduce qualitatively the observed profiles, we need to add the contribution coming from the continuum. Assuming that the continuum is not polarized and constant across the line, we have

$$\frac{X(\nu, \mathbf{\Omega})}{I(\nu, \mathbf{\Omega})} = \frac{\varepsilon^l_X(\nu, \mathbf{\Omega})}{\varepsilon^l_I(\nu, \mathbf{\Omega}) + \varepsilon^c_I} \ , \tag{15}$$

where $\varepsilon^c_I$ is the continuum contribution to the intensity of the emergent radiation, and where the apex " $l$ " is to recall that the corresponding quantity refers only to the line processes. In Appendix A we show and briefly discuss some results obtained by applying equation (13).

The Ba II D-lines that we are investigating are strong lines: according to theoretical models of the solar atmosphere the wings of these lines originate in the photosphere, while the line-cores in the high photosphere-low chromosphere. The optically thin slab model illuminated by the photospheric continuum that we are considering in this paper is therefore just a zero-order approximation. Nevertheless, it allows us to take into account in a very rigorous way the atomic physics involved in the problem, and to understand its essential role on the magnetic sensitivity of the polarization profiles of these lines, avoiding complications coming from radiation transfer effects. This is the first step of our investigation, in a forthcoming paper we will propose more realistic models, where radiation transfer effects will be taken into account.

Once the SEEs in the vertical reference system have been solved numerically, and the spherical statistical tensors have been rotated to the magnetic field reference system, we can calculate the emission coefficients for 90° scattering ($\theta = 90°$ and $\chi = 0°$ in Fig. 1) by means of equation (6), and the polarization of the scattered radiation through equation (15). In the following subsections we present our results for the Ba II $D_2$ and $D_1$ lines, for various magnetic field configurations.

### 4.1. *$D_2$ Line – No Magnetic Field Case: Origin of the Three Peaks Structure and Choice of Parameters Values*

As a first step, we observe the laboratory positions of the various HFS components of the $D_2$ line. The three isotopes without HFS contribute to the $D_2$ line with just one component each, those which have HFS contribute to this line with six components each, which may overlap. As seen in Figure 4 (right panel), it is possible to divide the various HFS components into three groups. The central group, at about 4554.03Å, is composed by the five components (three visible in the figure) due to the five isotopes without HFS (note that the main contribution comes from the isotope 138 because of its high abundance, while isotopes 130 and 132 bring a negligible contribution, not visible in the figure). The other components, due to the isotopes with HFS, fall at different wavelengths but can be gathered into two groups because of the large splitting of the ground level into the two $F = 1$ and $F = 2$ HFS levels (see Fig. 2). In particular, the group at about 4553.995Å is composed by the HFS components, of both isotopes 135 and 137, associated to the transitions towards the lower $F = 1$ HFS level, while the group at about 4554.045Å is composed by the HFS components associated to the transitions to the lower $F = 2$ HFS level. As we will see in more detail below, and as already pointed out by Stenflo (1997), the origin of the three peaks structure of the $D_2$ line lies in this splitting of the various components into these three groups. Similar considerations could be done about the position and relative strength of the

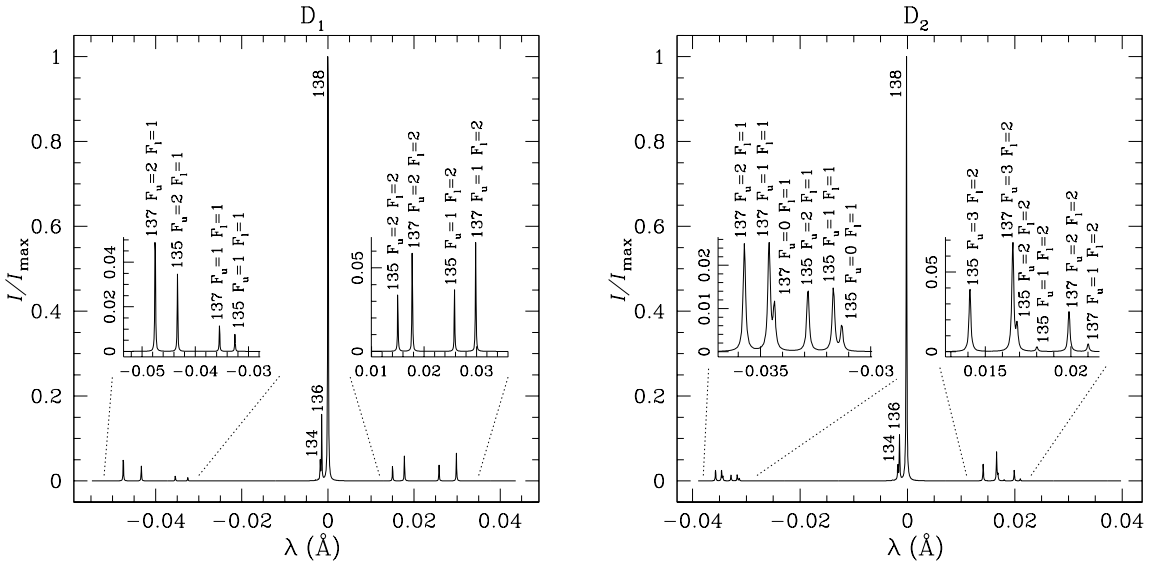


Fig. 4.— Laboratory positions of the various HFS components of the $D_1$ (left panel) and $D_2$ (right panel) lines resulting from the seven isotopes considered. The horizontal axis gives the wavelength (in Å) measured from 4934.075 Å for the $D_1$ line, and from 4554.029 Å for the $D_2$ line. These are the wavelengths (in air) of the isotope 138 $D_1$ and $D_2$ lines, respectively.

various components of the $D_1$ line, with the difference that now the upper level just has two HFS levels (instead of four).

Let us begin our analysis of the $D_2$ profile by considering only the isotope 138 (without HFS), and let us assume a Doppler width of 30 mÅ. For this isotope, as shown in the left panels of Figure 5, the ratio $\varepsilon_Q^l(\lambda)/\varepsilon_I^l(\lambda)$ (often referred to as fractional polarization) is constant and different from zero[6]. Adding the contribution of the continuum, the same ratio remains unchanged in the line-core (where $\varepsilon_I^l \gg \varepsilon_I^c$), while it goes to zero at the wavelengths corresponding to the wings of the intensity profile. The same considerations can be done for all the other isotopes without HFS. Let us consider now the isotope 137 (with HFS). For this isotope, assuming the same Doppler width, the profiles of the line emission coefficients $\varepsilon_I^l$ and $\varepsilon_Q^l$ show two peaks at the wavelength positions of the two groups of HFS transitions (see Fig. 5). The ratio $\varepsilon_Q^l(\lambda)/\varepsilon_I^l(\lambda)$ is no longer constant but decreases showing two broad minima at the wavelength positions corresponding to the wings of the $\varepsilon_I^l$ and $\varepsilon_Q^l$ profiles, and assumes the same value as the isotopes without HFS moving away from the line-core[7]. This

[6]See Appendix B for an analytical proof of this result.

[7]See Appendix B for an analytical proof of this result.

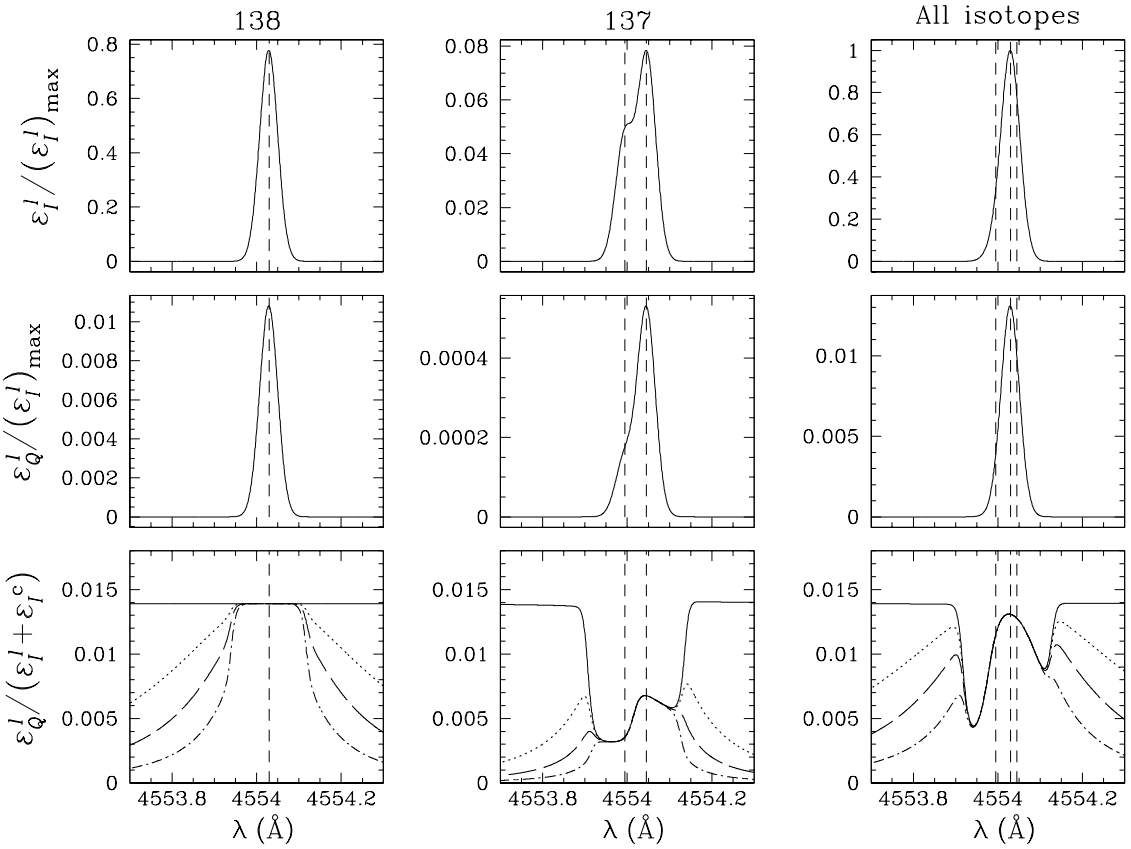


Fig. 5.— Theoretical profiles of the emission coefficients $\varepsilon_I^l(\lambda)$ and $\varepsilon_Q^l(\lambda)$, and of the ratio $\varepsilon_Q^l(\lambda)/(\varepsilon_I^l(\lambda)+\varepsilon_I^c)$, of the Ba II $D_2$ line, for the isotope 138, for the isotope 137 and for all the seven isotopes together, in the absence of a magnetic field. The emission profiles are normalized to the maximum value of the intensity emission profile, calculated taking into account the contribution of all the seven isotopes, $(\varepsilon_I^l)_{\max}$. The vertical dashed lines show the positions of the three groups of transitions (see text). The last row shows the $\varepsilon_Q^l(\lambda)/(\varepsilon_I^l(\lambda)+\varepsilon_I^c)$ profiles, without continuum (solid), with a continuum $\varepsilon_I^c/(\varepsilon_I^l)_{\max}$ of $10^{-5}$ (dot), of $3\times10^{-5}$ (long dash), and of $9\times10^{-5}$ (dash-dot).

profile clearly shows the depolarizing effect of the HFS. The role of the continuum is the same as observed for the isotopes without HFS. The same arguments hold for the isotope 135.

This investigation on the isotopes 138 and 137 shows that the central peak of the observed $Q/I$ profile is due to the isotopes without HFS, while the two secondary peaks are due to the isotopes with HFS. The position and amplitude of these secondary peaks appear to be strongly dependent on the background continuum emissivity $\varepsilon_I^c$, a physical quantity that,

given the exploratory character of this paper, we will just parametrize in order to reproduce at best the observed profile.

We consider now all the isotopes together and we adjust the Doppler width, the anisotropy factor and the continuum intensity in order to obtain the best fit to the $Q/I$ profile observed by Stenflo & Keller (1997), still assuming that no magnetic field is present. Changing the Doppler width we can modify the separation between the two minima of the profile $\varepsilon^l_Q(\lambda)/\varepsilon^l_I(\lambda)$. To obtain the same separation as the observed profile we need a value of about 30 mÅ. This value seems to be very reasonable as it can be obtained assuming a temperature of about 6000 K and a microturbulent velocity of about 1.8 km/s, values which are in good agreement with those given by semi-empirical chromospheric models at the height of about 1000 km.

Modifying the anisotropy factor we simply scale the ratio $\varepsilon^l_Q(\lambda)/\varepsilon^l_I(\lambda)$. Radiative transfer effects are disregarded in our model and, since the Ba II $D_2$ line is a strong line, we can expect that the calculated value for the anisotropy factor taking into account only the photospheric continuum (see § 2.3), is probably overestimated. We find indeed that the anisotropy factor has to be decreased to the value of 0.037 (approximately 1/5 of the value 0.176 mentioned in § 2.3) to obtain the observed value of the ratio $Q/I$ at the wavelength position of the central peak.

In this paper we are not taking into account the continuum processes in a rigorous way. As mentioned above, we describe the effect of the continuum simply through the parameter $\varepsilon^c_I$. As shown in Figure 5, the continuum modifies the wings of the profile. Taking as a reference the "red" secondary peak of the observed profile, we find that the best fit is obtained assuming a value for $\varepsilon^c_I/(\varepsilon^l_I)_{\max}$ of $9 \times 10^{-5}$. With these values of the parameters, applying equation (15), we get the profile shown in the panel b of Figure 6 which reproduces quite well the observed profile, and which is very similar to a theoretical profile already obtained by Stenflo (1997).

The main aim of this work is to investigate the magnetic sensitivity of the linear and circular polarization of the D-lines of Ba II, and not merely to reproduce as better as possible the observed profiles of these lines. For this reason, we prefer to perform our investigation by sticking to the values of the parameters found for the simpler, unmagnetized case. Obviously there is no reason to think that the best agreement with the observed profile has to be found in the absence of a magnetic field. It is likely enough that the best agreement could be obtained in the presence of a deterministic or microturbulent magnetic field, using different values of the parameters. For example, in panels c and d of Figure 6 we show the best theoretical profiles that we have obtained in the presence of a microturbulent magnetic field of 5 G and a vertical magnetic field of 40 G, choosing different values of the free parameters (see caption to Fig. 6).

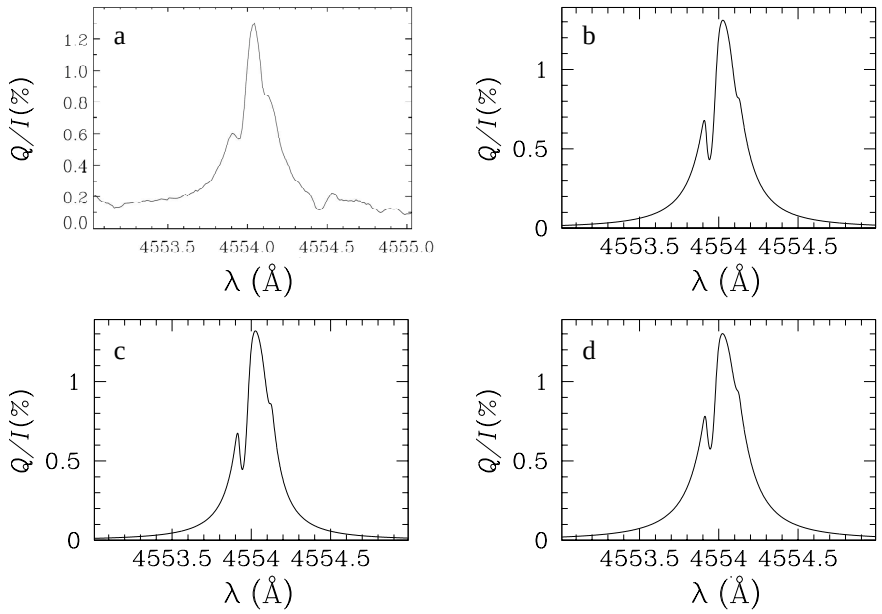


Fig. 6.— *Panel* a: observed $Q/I$ profile of the Ba II $D_2$ line (Stenflo & Keller 1997). *Panel* b: theoretical $Q/I$ profile obtained in the absence of a magnetic field, choosing a Doppler width ($\Delta\lambda_D$) of 30 mÅ, an anisotropy factor ($w$) of 0.037, and a continuum $\varepsilon_I^c/(\varepsilon_I^l)_{\rm max}$ of $9 \times 10^{-5}$. *Panel* c: theoretical $Q/I$ profile obtained in the presence of a microturbulent magnetic field of 5 G, choosing the following values of the free parameters: $\Delta\lambda_D$=30 mÅ, $w$=0.052, $\varepsilon_I^c/(\varepsilon_I^l)_{\rm max}$=$1.77 \times 10^{-4}$. *Panel* d: theoretical $Q/I$ profile obtained in the presence of a vertical magnetic field of 40 G, choosing the following values of the free parameters: $\Delta\lambda_D$=30 mÅ, $w$=0.037, $\varepsilon_I^c/(\varepsilon_I^l)_{\rm max}$= $7.5 \times 10^{-5}$.

### 4.2. *$D_2$ Line – The Influence of a Magnetic Field on the Emergent Polarization*

Depending on its strength, and on its direction with respect to the local vertical and to the direction of the scattered radiation, a magnetic field will differently modify the linear and circular polarization of the line through the Zeeman and the Hanle effects[8]. It is well known that the Zeeman effect produces in general elliptical polarization, which degenerates into linear polarization if the magnetic field lies on the plane perpendicular to the line-of-sight (LOS), and into circular polarization if the magnetic field lies along the LOS. The Zeeman effect dominates the polarization of the scattered radiation if the splitting among

[8]Hereafter, regardless of the particular regime (Zeeman effect regime, incomplete or complete Paschen-Back effect regime), any polarization signal that originates from the splitting among the magnetic sublevels will be referred to as Zeeman effect.

the magnetic sublevels is of the same order of magnitude or larger than the Doppler width of the line. This criterion gives a critical value of the magnetic field strength for the Ba II $D_2$ line of about 3000 G. However, if the magnetic field is not too weak, and if there are no other mechanisms that dominate the polarization, it is possible to identify Zeeman effect signatures on the fractional polarization profiles even for intensities much smaller than the critical value. As we will see below in Figures 7 and 8, for the line under investigation magnetic fields of about 50 G are enough in order the transverse Zeeman effect to produce appreciable modifications of the linear polarization signal.

On the other hand, as described in § 3, a magnetic field is able to modify the atomic polarization, and therefore the polarization of the scattered radiation. Depending on the configuration of the magnetic field, and on the geometry of the scattering event, different signatures of the Hanle effect can be produced on the polarization profiles. As the observed scattering polarization in the Ba II $D_2$ line is dominated by the atomic polarization of the upper level, recalling that for the $^2P_{3/2}$ level $t_{\rm life} \approx 1/A_{u\ell} \approx 10^{-8}$ s and $g_{\rm L} = 1.33$, applying equation (10), we find that the line is expected to be sensitive to the Hanle effect for magnetic field strengths ranging approximately between 1 G and 100 G (values which are smaller than the ones needed for the transverse Zeeman effect to be appreciable).

### 4.3. *$D_2$ Line – Vertical Magnetic Field*

In this section we consider the effect of a vertical magnetic field on the theoretical $Q/I$ profile[9] of Figure 6 (panel b). The results are shown in Figure 7. The first interesting feature is the enhancement of the linear polarization at the wavelength positions of the two dips between the line-core peak and the two secondary peaks, for magnetic fields relatively weak (less than 50 G), for which the influence of the transverse Zeeman effect is negligible. In order to understand which physical mechanism is at the origin of this and other features shown by these $Q/I$ profiles, in the various ranges of magnetic field intensity, we try to distinguish which polarization properties of the emergent radiation are due to the atomic polarization effects and which ones are due to the Zeeman effect. To this aim, we can obtain interesting information by plotting the profiles obtained through equation (15) according to two different strategies:

A) taking the nominal values for the spherical statistical tensors, but setting $B = 0$ when calculating the energy eigenvalues and eigenvectors,

[9]Hereafter by 'theoretical $Q/I$ profile' we will always refer to the profile obtained by applying equation (15).

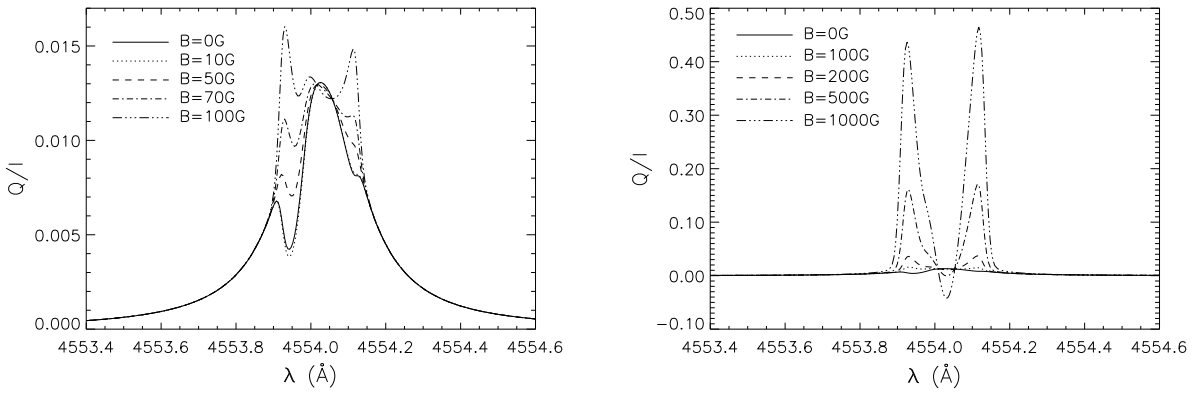


Fig. 7.— Theoretical $Q/I$ profile of the Ba II $D_2$ line in the presence of a vertical magnetic field ($\theta_B = 0°$). In the left panel the magnetic field varies between 0 and 100 G while in the right panel it varies between 0 and 1000 G. Note the difference in the scale of the two figures.

B) setting equal to zero all the spherical statistical tensors, except $\rho^0_0$, but taking properly into account the influence of $B$ on the energy eigenvalues and eigenvectors.

In the former case (Fig. 8, middle column) we are taking into account only the effects due to atomic polarization, neglecting the Zeeman effect, while in the latter case (Fig. 8, right column) we are taking into account only this second effect, within the framework of the Paschen-Back effect theory.

From Figure 8, it is clear that the above-mentioned enhancement of the linear polarization at the wavelength positions of the dips, in the presence of a weak vertical magnetic field, is not due to the Zeeman effect, but to the Hanle effect acting only on the isotopes with HFS (see § 4.1). We note in fact that the central peak, which is due to the isotopes without HFS is not sensitive, in this range, to the magnetic field. Actually this particular behaviour can be explained in terms of two different mechanisms: the anti-level-crossing effect (briefly introduced in § 2.1), and the change of coupling scheme of the atomic system[10]. We note first that if the magnetic field lies along the symmetry axis of the radiation field, only the statistical tensors $\rho^0_0$ and $\rho^2_0$ are different from zero (see also § 2.3). As the incomplete Paschen-Back effect regime is reached, the HFS magnetic sublevels with the same $f$ quantum number separate from each other (see § 2.1), as a consequence the terms $\rho^2_0(F, F')$ (which quantifies the corresponding quantum interferences) decrease, and this causes an increase of the polarization of the scattered radiation (anti-level-crossing-effect, see LL04 for details).

[10]According to our definition, these effects should be better considered as particular cases of the Hanle effect.

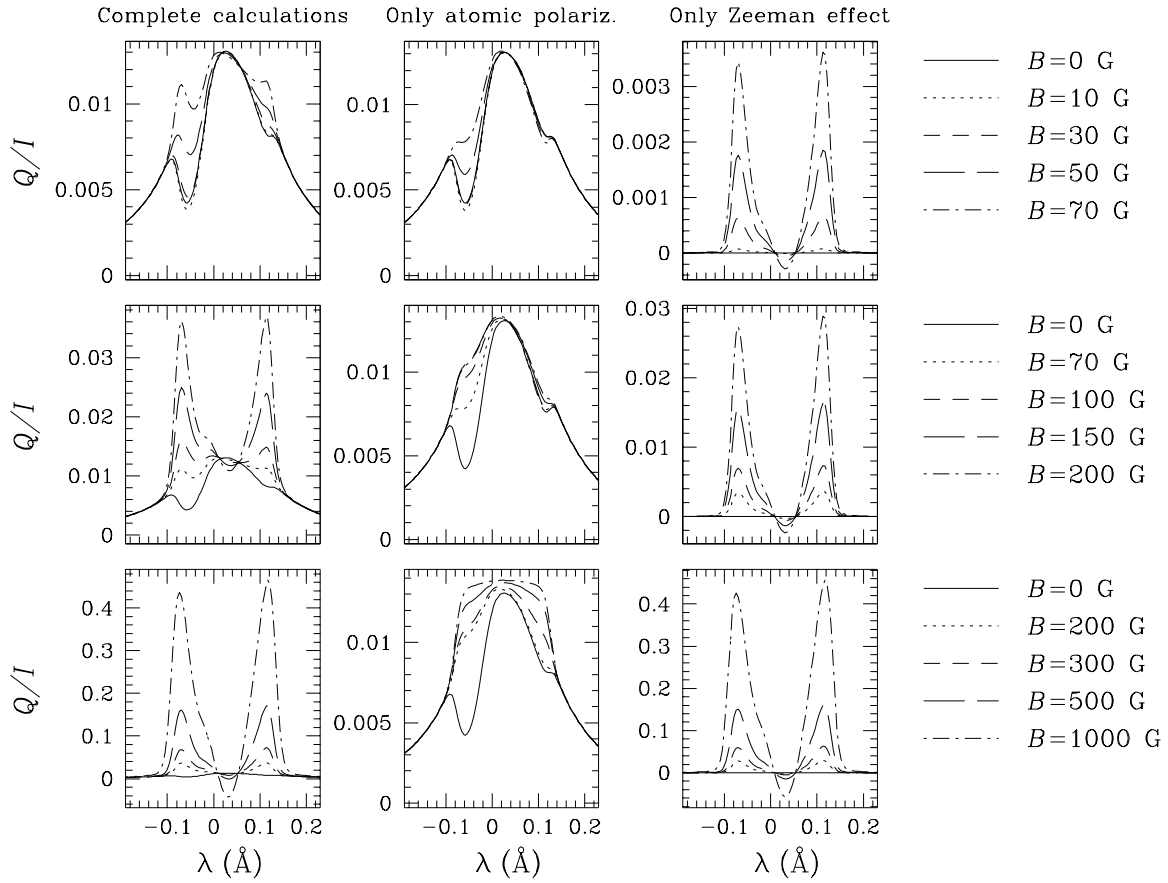


Fig. 8.— *Left column*: theoretical $Q/I$ profiles of the Ba II $D_2$ line obtained in the presence of a vertical magnetic field. *Middle column*: theoretical $Q/I$ profiles obtained neglecting the Zeeman effect (only atomic polarization effects). *Right column*: theoretical $Q/I$ profiles obtained neglecting atomic polarization effects (only Zeeman effect). The zero of the wavelength scales is taken at 4554 Å.

On the other hand, as already stated in § 2.1, going from the Zeeman effect regime to the complete Paschen-Back effect regime, the magnetic field produces an energy eigenvectors basis transformation. This transformation implies a changing of the coupling scheme of the atomic system, which affects the polarization state of the atomic system[11]. Both these mechanisms begin to play an appreciable role as the upper level of the $D_2$ enters the incomplete Paschen-Back effect regime. The order of magnitude of the magnetic field strength needed to reach this regime can be estimated from the relation $0.1 \leq \Delta\lambda_B/\Delta\lambda_{\rm hfs} \approx 1$, where $\Delta\lambda_B$ is the splitting induced by the magnetic field, and $\Delta\lambda_{\rm hfs}$ is the wavelength separation

[11]The complex mechanism of inhibition of atomic polarization transfer discussed in Casini et al. (2002) is a particular consequence of this coupling scheme transformation.

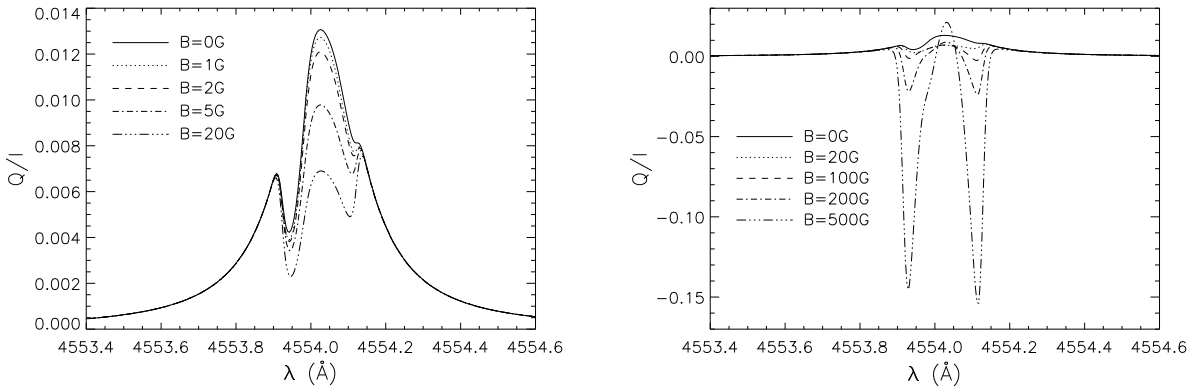


Fig. 9.— Theoretical $Q/I$ profiles of the Ba II $D_2$ line in the presence of a horizontal magnetic field, perpendicular to the line of sight ($\theta_B = 90°$, $\chi_B = \pm 90°$)

between the HFS $F$-levels. Applying this relation to the Ba II $D_2$ line, we find that this effect is expected to take place for magnetic fields larger than 10 G, as it is observed in Figure 8. The possibility of an enhancement of the scattering polarization in the presence of a vertical magnetic field, through this kind of mechanisms, was already pointed out by Trujillo Bueno et al. (2002) for the case of the Na I $D_2$ line.

Increasing the magnetic field strength, the transverse Zeeman effect eventually becomes appreciable and, besides the previous effect, we see an increase of the polarization at the wavelength position of the two peaks on the wings of the profile (see Fig. 7 and Fig. 8). Going to magnetic fields of about 200 G or stronger we enter the transverse Zeeman effect regime, and the linear polarization profile takes the typical symmetrical shape[12] (see Fig. 7 and Fig. 8).

### 4.4. *$D_2$ Line – Horizontal Magnetic Field, Perpendicular to the Line of Sight*

In the presence of a weak horizontal magnetic field, perpendicular to the line of sight, as the field increases we observe a decrease of the linear polarization at the wavelength position of the central peak, due to the Hanle effect. However, consistently with the fact that the Hanle effect has to vanish in the far wings of the line, the two peaks on the wings remain almost unaffected, as can be seen in the left panel of Figure 9. Similarly to what happens in the presence of a vertical magnetic field, going to intensities of about 50 G or stronger we enter the transverse Zeeman effect regime, and the $Q/I$ profile takes the well known shape

[12]Note that here we are plotting the ratio $\varepsilon_Q(\lambda)/\varepsilon_I(\lambda)$ and not just $\varepsilon_Q(\lambda)$.

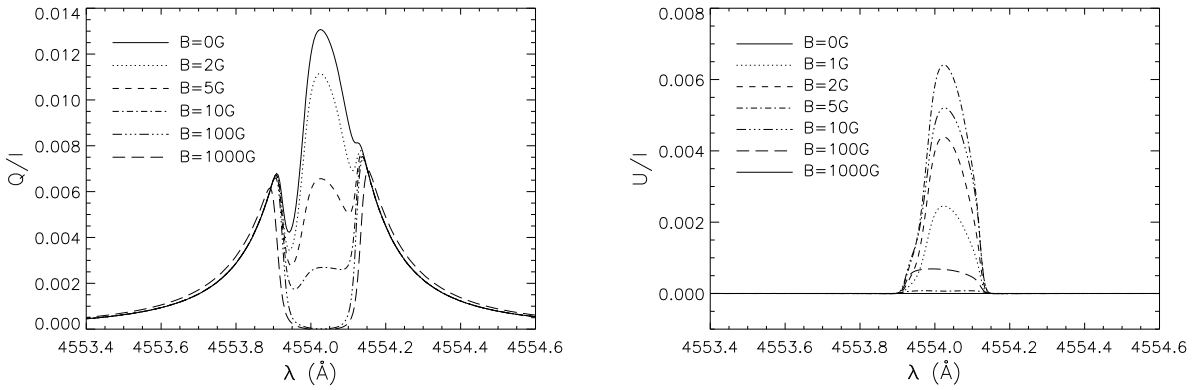


Fig. 10.— Theoretical $Q/I$ (left panel) and $U/I$ (right panel) profiles of the Ba II $D_2$ line in the presence of a longitudinal magnetic field ($\theta_B = 90°$, $\chi_B = 0°$). For $\chi_B = 180°$ the $U/I$ profile would be the same except for an overall sign switch.

shown in the right panel of Figure 9.

### 4.5. *$D_2$ Line – Horizontal Magnetic Field, Directed Along the Line of Sight*

In the presence of a longitudinal magnetic field of increasing strength, there is again a decrease of the linear polarization at the wavelength position of the central peak, due to the Hanle effect, while the two peaks on the wings are not affected. In this geometry the Zeeman effect does not modify the linear polarization and, going to stronger magnetic fields, we enter a regime of saturation, as shown in the left panel of Figure 10. Because of the Hanle effect, we have in this case a rotation of the plane of linear polarization. This implies the presence of the non zero $U/I$ signal shown in the right panel of Figure 10. Finally we have a typical antisymmetric $V/I$ signal due to the longitudinal Zeeman effect, as shown in Figure 11. For weak magnetic fields (of the order of about 100 G or weaker) the signal increases linearly with the magnetic field strength. Going to stronger fields the linearity is slowly lost, and the profile starts to saturate.

### 4.6. *$D_2$ Line – Random-Azimuth Magnetic Field*

In this section we present the results obtained for the fractional polarization in the presence of magnetic fields with a given inclination and a random azimuth (i.e. the results obtained in the presence of a magnetic field of given strength and inclination, averaged over

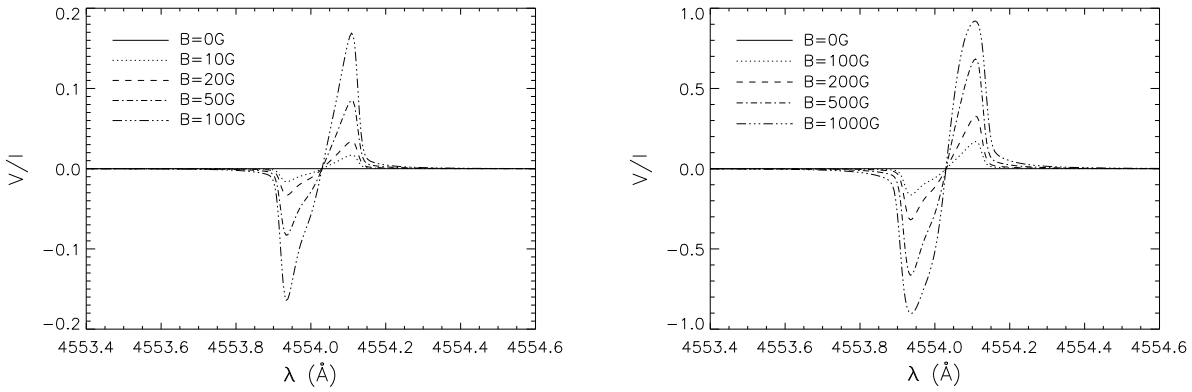


Fig. 11.— Theoretical $V/I$ profiles of the Ba II $D_2$ line in the presence of a longitudinal magnetic field.

the azimuth). Figure 12 shows the theoretical profiles obtained in the presence of random-azimuth magnetic fields with inclinations of 30°, 60° and 90°. In the 30° case we observe that increasing the magnetic field strength the linear polarization decreases at the wavelength position of the central peak and of the two dips close to it, because of the Hanle effect. For magnetic fields of about 100 G it is possible to observe the first signatures of the Zeeman effect, which dominates the linear polarization as we further increase its intensity. Note that as the main component of the magnetic field is vertical, the Zeeman effect produces the typical three lobes profiles with the same signs as in the case of a deterministic vertical magnetic field. Similar considerations hold for a random-azimuth magnetic field with an inclination of 60° and 90°. As the main component of the magnetic field is now horizontal, as far as the Zeeman effect starts to dominate the polarization (which happens for fields of about 200 G or stronger in the 60° case, and for fields of about 50 G or stronger in the 90° case), we obtain the well known Zeeman effect profiles with the same signs as in the case of a deterministic horizontal magnetic field, perpendicular to the LOS. Stronger magnetic fields are needed for the Zeeman effect to be appreciable in the presence of a random-azimuth magnetic field with an inclination of 60° because in this case the vertical and the horizontal components of the magnetic field (which produce Zeeman effect profiles with opposite signs) are comparable.

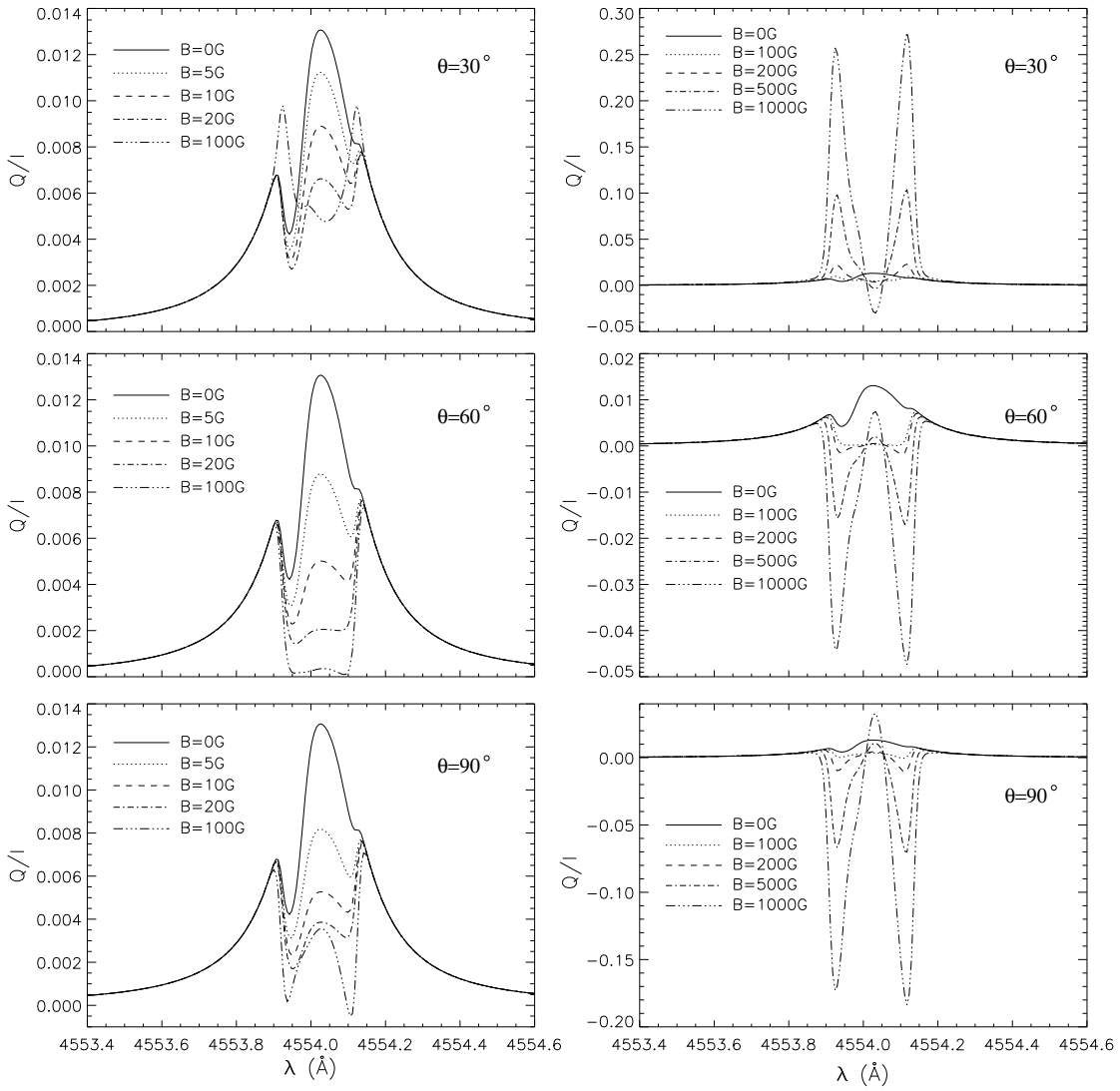


Fig. 12.— Theoretical $Q/I$ profiles of the Ba II $D_2$ line in the presence of a random-azimuth magnetic field for three different inclinations: 30° (top), 60° (middle), and 90° (bottom).

### 4.7. *$D_2$ Line – Microturbulent Magnetic Field*

Averaging the emission coefficient over all the possible orientations of the magnetic field[13], we can investigate the polarization properties of the line in the presence of a unimodal microturbulent magnetic field. As shown in Figure 13, we observe that the linear polarization

[13]See Appendix C for the details implied in performing this average.

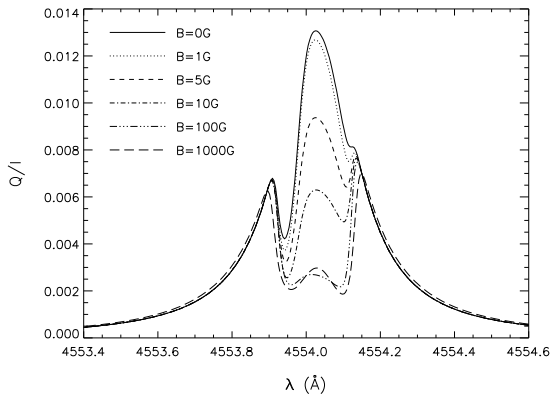


Fig. 13.— Theoretical $Q/I$ profiles of the Ba II $D_2$ line in the presence of a microturbulent magnetic field.

at the wavelength position of the central peak decreases, while the two peaks on the wings remain constant as the magnetic field strength is increased. This behaviour can be easily understood: in the presence of a microturbulent magnetic field there is no observational polarization signal due to the Zeeman effect, while the Hanle effect produces a decrease of the linear polarization only in the line-core. For $B > 100$ G, we enter a saturation regime and, contrary to the case of a longitudinal field, we still have a non-zero signal in the line-core.

### 4.8. *The Polarization of the $D_1$ Line*

To understand the physical origin of the polarization signal observed in the $D_1$ line and, in particular, the role of HFS, we start our investigation considering separately the isotopes 138 (without HFS) and 137 (with HFS), before taking into account the contribution coming from all the seven isotopes together. We use the values of the average number of photons and of the anisotropy factor given in § 2.3, and a Doppler width of 30 mÅ. In Figure 14 we can see that the emission coefficient $\varepsilon_Q^l$ of the isotopes without HFS is constant in wavelength and equal to zero, while it shows an anti-symmetrical profile, that goes rapidly to zero moving away from the line-core, in the isotopes with HFS. For these isotopes the frequency integrated Stokes $Q$ emission coefficient is equal to zero[14]. The profile of the ratio $\varepsilon_Q^l/\varepsilon_I^l$ of the isotopes with HFS, contrary to the case of the $D_2$ line, goes slowly to zero moving away from the line-core. For this reason the effect of the continuum is less important in this line, as it just 'pushes' more rapidly to zero the wings of this profile without modifying significantly

[14]All these properties can be derived analytically, and are briefly discussed in Appendix B.

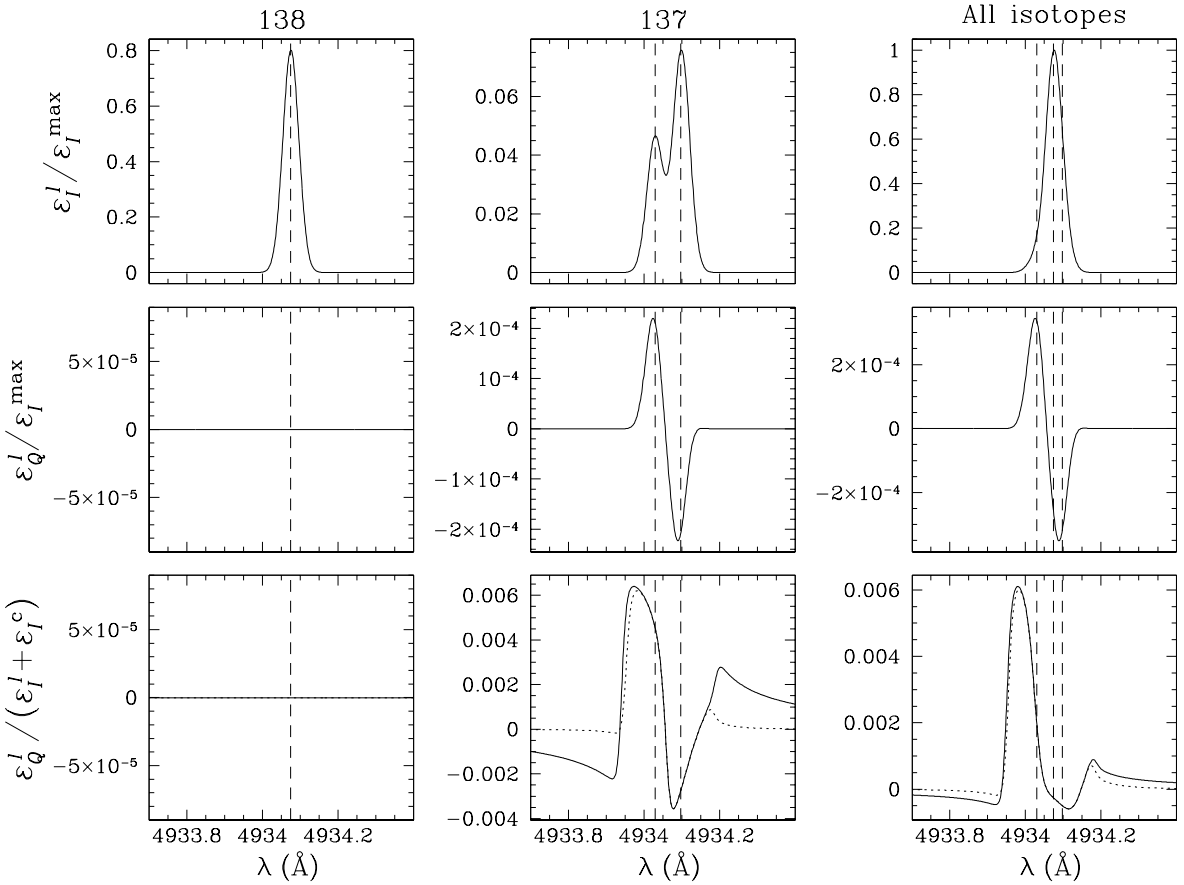


Fig. 14.— Theoretical profiles of the emission coefficients $\varepsilon_I^l(\lambda)$ and $\varepsilon_Q^l(\lambda)$, and of the ratio $\varepsilon_Q^l(\lambda)/(\varepsilon_I^l(\lambda)+\varepsilon_I^c)$, of the Ba II $D_1$ line, for the isotope 138, for the isotope 137 and for all the seven isotopes together, in the absence of a magnetic field. The emission profiles are normalized to the maximum value of the intensity emission profile, calculated taking into account the contribution of all the seven isotopes, $(\varepsilon_I^l)_{\max}$. The vertical dashed lines show the positions of the three groups of transitions (see § 4.1). The last row shows the $\varepsilon_Q^l(\lambda)/(\varepsilon_I^l(\lambda)+\varepsilon_I^c)$ profiles without continuum (solid), and with a continuum $\varepsilon_I^c/(\varepsilon_I^l)_{\max}$ of $9\times10^{-5}$ (dot).

its shape. In the following description of our investigation on the magnetic sensitivity of this line we have neglected the contribution to the intensity coming from the continuum.

As seen in Figure 14, within the framework of our modeling approach for weak magnetic fields ($B < 50$ G) it is not possible to obtain the symmetric $Q(\lambda)/I(\lambda)$ profile observed by Stenflo et al. (2000). The theoretical profile that we have obtained has no evident symmetries, and its main peak does not coincide in wavelength with the central peak of the observed profile. Changing the Doppler width and the anisotropy factor we can modify the width and the amplitude of the peaks, adding a continuum contribution to the $Q$ Stokes parameter we

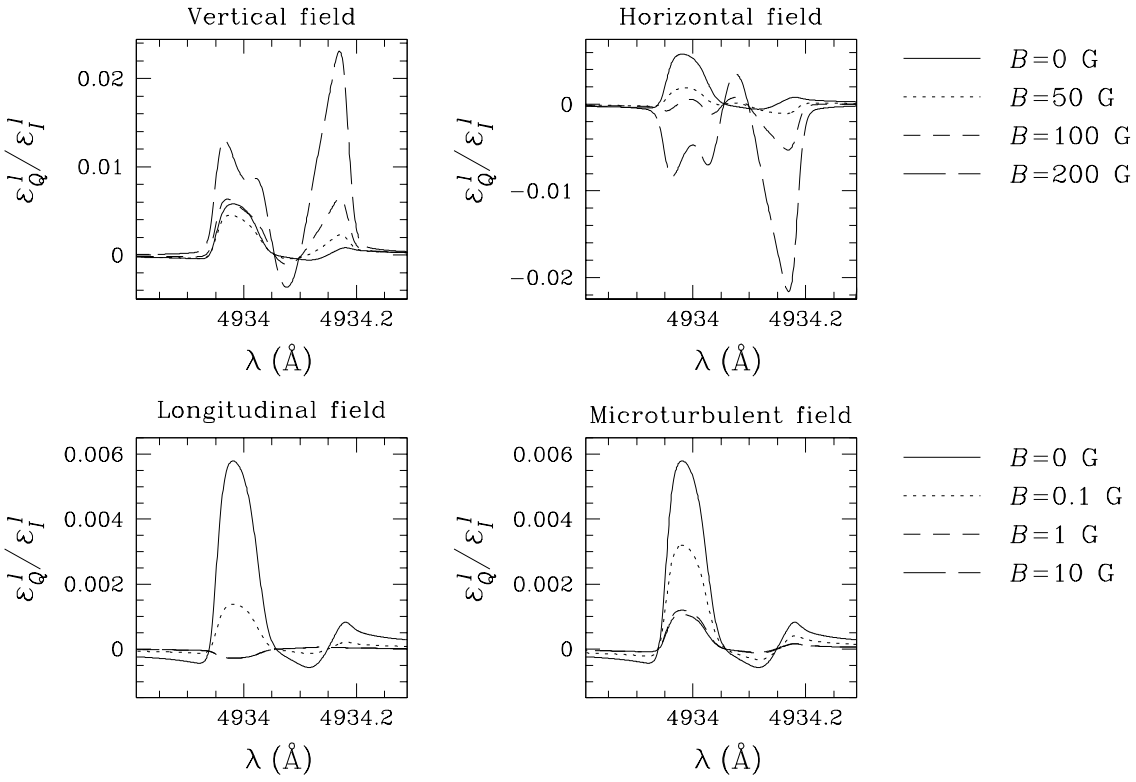


Fig. 15.— Theoretical profiles for the ratio $\varepsilon_Q^l/\varepsilon_I^l$ of the Ba II $D_1$ line, in the presence of a vertical, horizontal perpendicular to the line-of-sight, longitudinal and microturbulent magnetic field of various intensities.

can shift the profile along the polarization scale in order to get values of $Q/I$ in the wings close to the observed ones, but we cannot really modify the shape of the profile. In Figure 15 we show the theoretical $\varepsilon_Q^l/\varepsilon_I^l$ profiles in the presence of a vertical, horizontal perpendicular to the line-of-sight, longitudinal and microturbulent magnetic field. In complete analogy with the $D_2$ line, the profiles are modified by the combined action of the Hanle and Zeeman effects. As already pointed out by Trujillo Bueno et al. (2002) and by Casini et al. (2002) for the Na I $D_1$ line case, it appears that, at this level of approximation, the only way to get a symmetric profile, centered at the wavelength position of the central peak of the observed profile (see Stenflo et al. 2000), is to be in the presence of a magnetic field strong enough to enter the transverse Zeeman effect. However, as expected, the transverse Zeeman effect produces in the $\varepsilon_Q^l/\varepsilon_I^l$ profile two wing lobes that are more significant than the central one, which is not the case of the observed profile.

## 5. CONCLUSIONS

The most interesting general conclusion of our theoretical investigation on the magnetic sensitivity of the D-lines of Ba II is that the observation and modeling of the Hanle and Zeeman effects in these resonance lines provide a novel diagnostic tool for mapping the magnetic fields of the upper photosphere and lower chromosphere.

In particular, the Ba II $D_2$ line at 4554 Å is particularly interesting because the emergent linear polarization has contributions from different isotopes, contributions that are easily resolved and have a different behavior in the presence of a magnetic field. As a result, there is a differential magnetic sensitivity of the emergent linear polarization at line center (where the signal is produced by the even isotopes without HFS) with respect to the line wings (where the signals are produced by the odd isotopes with HFS). For instance, for the case of a vertical magnetic field with a strength between 10 G and 100 G, approximately, only the isotopes with HFS are sensitive to the Hanle effect, which produce an enhancement of the scattering polarization at the two $Q/I$ wing wavelengths. For the case of a horizontal field between about 1 and 100 G the most conspicuous observable effect is the line core depolarization produced by the Hanle effect of the barium isotopes devoid of HFS. In both cases, the transverse Zeeman effect begins to play an increasingly dominating role for field intensities larger than 100 G, approximately. Useful information on the magnetic sensitivity of the $Q/I$ profile of the calculated emergent radiation in the $D_2$ line can be seen in Figure 12, which corresponds to the case of a random azimuth magnetic field with a fixed inclination. Of particular interest is the case of an unimodal microturbulent and isotropic magnetic field (see Figure 13), for which there is no contribution from the Zeeman effect and Stokes $U$ and $V$ are zero.

Concerning the enigmatic Ba II $D_1$ line it is important to note that in the absence of magnetic fields only the 18% isotopes with HFS are capable of producing linear polarization through bound-bound transitions. As with the sodium $D_1$ line, this is possible thanks to the fact that in the absence of depolarizing mechanisms only the upper and lower levels of the $D_1$ line transition in the odd isotopes are significantly polarized. Interestingly, a $Q/I$ profile with a conspicuous blue-shifted peak is obtained if only the selective emission of polarization components that results from the upper-level polarization are taken into account (see the last panel of the third row of Fig. 14)[15]. Under such circumstances one could argue that a detailed radiative transfer solution for the Ba II $D_1$ line including the Doppler shifts caused by the convective motions and waves that are present in the solar

[15]Note, however, that in the absence of a magnetic field the theoretical $Q/I^{max}$ profile of the Ba II $D_1$ line (see the last panel in the second row of Fig. 14) has an antisymmetrical shape, as already found for the Na I $D_1$ line (see Fig. 2 in Trujillo Bueno et al. 2002), when only selective emission processes are considered.

atmospheric plasma could perhaps produce a symmetric $Q/I$ profile for the Ba II $D_1$ line, as observed by Stenflo et al. (2000). However, as shown in this paper, for the Ba II $D_1$ line we should expect also a significant contribution from "zero-field" dichroism –that is, from the selective absorption of polarization components that results from the lower-level polarization. In fact, when both selective emission and absorption processes are taken into account through the approximation of equation (13), we then obtain the nearly antisymmetric $Q/I$ profile of Figure 18. Note that there is no possibility of destroying the lower level polarization without simultaneously destroying the atomic polarization of the upper level of the $D_1$ line (see Fig. 1 of Trujillo Bueno et al. 2002, and our Fig. 3 for barium levels). As far as dichroism is neglected, within the framework of our present modeling assumptions one might then be tempted to conclude that the only possibility of obtaining a symmetric $Q/I$ peak for the Ba II $D_1$ line is via the transverse Zeeman effect, even though, through this kind of mechanism, a profile with wing lobes more significant then the central one is obtained, and magnetic fields quite intense are needed. Our approach neglects, however, the radiative transfer effects that we certainly have in the real solar atmosphere, with its vertical stratification, horizontal inhomogeneities and the Doppler shifts caused by the above-mentioned upflows, downflows and waves. Therefore, detailed radiative transfer simulations using realistic solar atmospheric models are urgently needed in order to be able to conclude whether a symmetric $Q/I$ profile for the Ba II $D_1$ line with a significant line-center peak may be obtained within the framework of the density matrix theory we have applied in this paper, either because of the influence of the atomic level polarization of the 18% of the barium isotopes endowed of HFS (which would require the presence of atmospheric regions with very weak fields), or due to the transverse Zeeman effect of all the barium isotopes (which would require the presence of a sufficiently strong magnetic field, and the absence of significant saturation effects at the line-center wavelength).

Finally, we would like to finish this paper by emphasizing the importance of pursuing high-spatial resolution polarimetric observations of the Ba II $D_2$ line (e.g., via Fabry-Perot polarimetry) in order to help decipher the spatial and temporal fluctuations of the magnetic field vector, in both active and quiet regions of the solar atmosphere.

This research has been partially funded by the European Commission through the Solar Magnetism Network, and by the Spanish Ministerio de Educación y Ciencia through project AYA2004-05792.

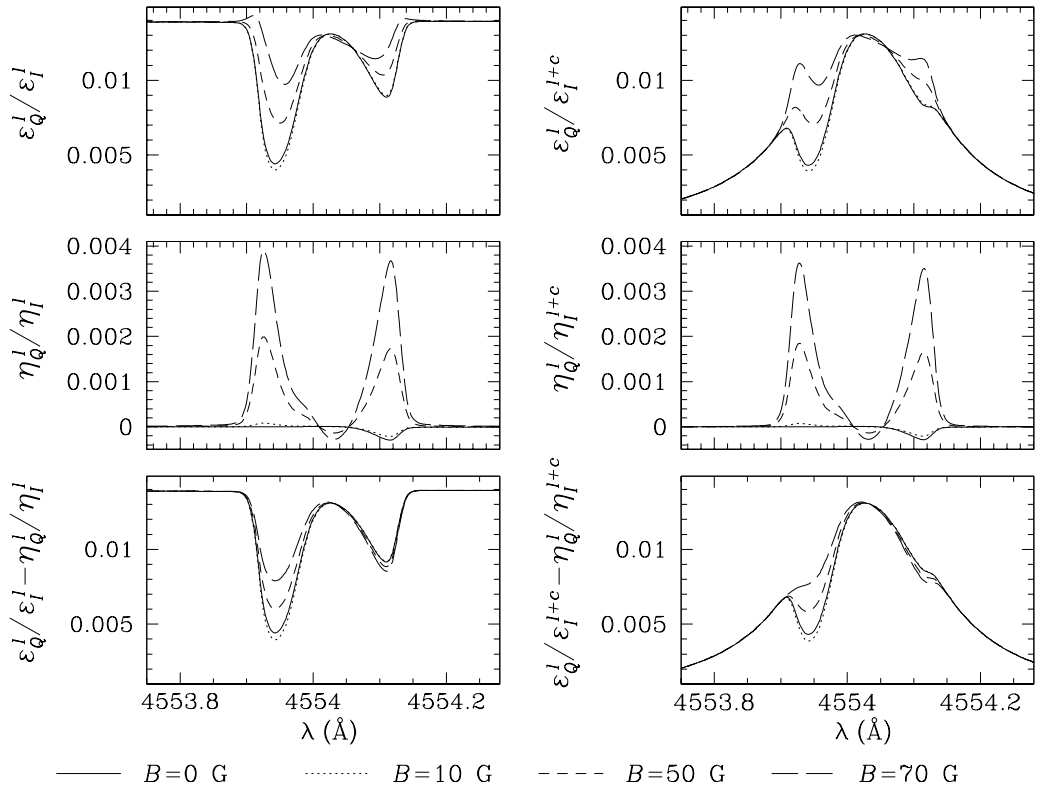


Fig. 16.— *Left column:* theoretical profiles for the ratios (from the top) $\varepsilon_Q^l/\varepsilon_I^l$, $\eta_Q^l/\eta_I^l$ and for their difference, in the presence of a vertical magnetic field of various intensities. *Right column:* line profiles taking into account the continuum contribution to the intensity emission and absorption ($\varepsilon_I^c/(\varepsilon_I^l)_{\rm max} = 9 \times 10^{-5}$, $\eta_I^c$ calculated through eq. [A2]). Calculations refer to the Ba II $D_2$ line.

## A. RESULTS OBTAINED TAKING INTO ACCOUNT DICHROISM EFFECTS

We show here the results obtained taking into account the absorption effects in the $D_2$ line. Including the contribution of the continuum, equation (13) takes the form

$$\frac{X(\nu,\mathbf{\Omega})}{I(\nu,\mathbf{\Omega})} \approx \frac{\varepsilon_X^l(\nu,\mathbf{\Omega})}{\varepsilon_I^l(\nu,\mathbf{\Omega})+\varepsilon_I^c} - \frac{\eta_X^l(\nu,\mathbf{\Omega})}{\eta_I^l(\nu,\mathbf{\Omega})+\eta_I^c} \quad , \tag{A1}$$

where $\eta_I^c$ is the continuum contribution to the total intensity absorption. This quantity can be calculated from the continuum intensity emission coefficient through the relation

$$\eta_I^c = \frac{\varepsilon_I^c}{B_{\rm P}(\nu_0, T=5800K)} \quad , \tag{A2}$$

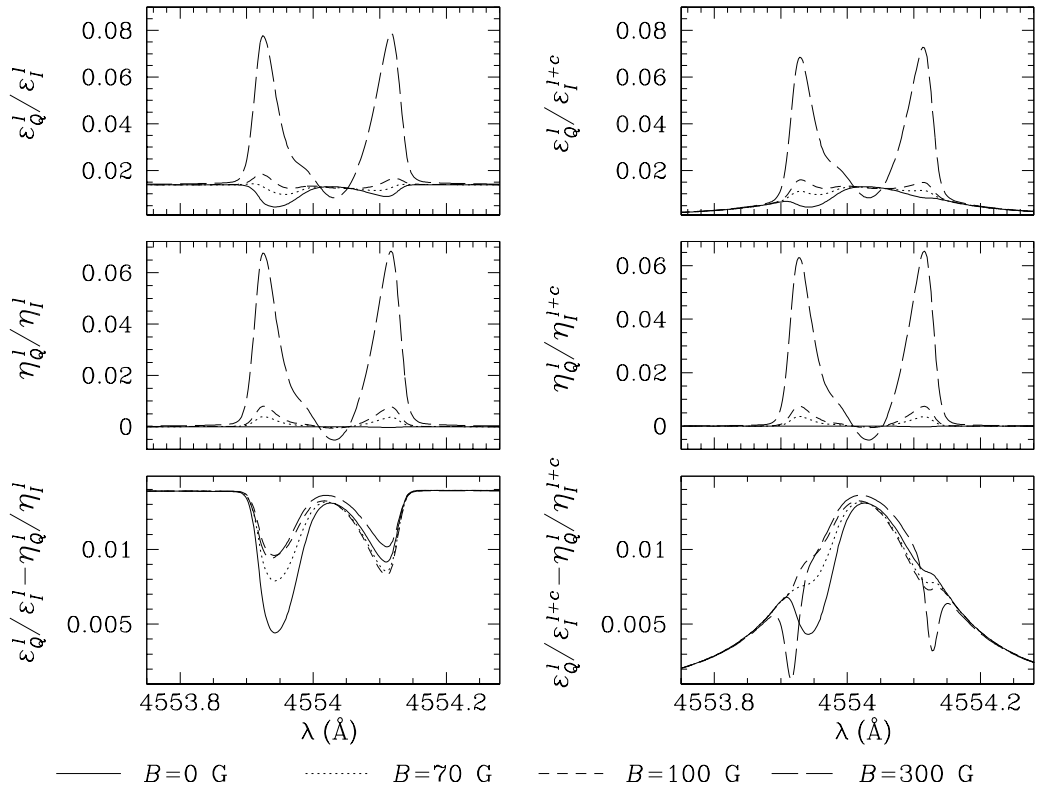


Fig. 17.— Same as Figure 16 for larger values of the magnetic field.

where $B_{\rm P}(\nu_0, T = 5800K)$ is the Planck function calculated at the central wavelength ($\nu_0$) of the line we are investigating and at the effective solar temperature. Figures 16 and 17 show the results for the $D_2$ line. We consider first the results obtained without continuum. In the absence of magnetic fields, since the atomic polarization in the lower level is much smaller than in the upper level of $D_2$ (see Fig. 3), the absorption effects are completely negligible, as already observed in § 4. Introducing a vertical magnetic field the profile of the ratio $\eta_Q^l/\eta_I^l$ is modified by the transverse Zeeman effect and, as the magnetic field is increased, it assumes a shape which is very similar to the one observed for $\varepsilon_Q^l/\varepsilon_I^l$ (see Fig. 17). For this reason, the profile obtained through equation (13) does not show any detail due to the transverse Zeeman effect since the contribution coming from emission and absorption cancel out. The situation is somewhat different in the presence of the continuum. In this case, as shown in Figure 17, for magnetic fields stronger than about 100 G the contribution coming from the absorption term becomes more important. At this point it is important to remember that the continuum has been considered as a parameter in our investigation and, as stressed in § 4.1, we have to be careful when dealing with spectral details that find their origin in this physical aspect of the problem. Similar considerations can be done for the other magnetic

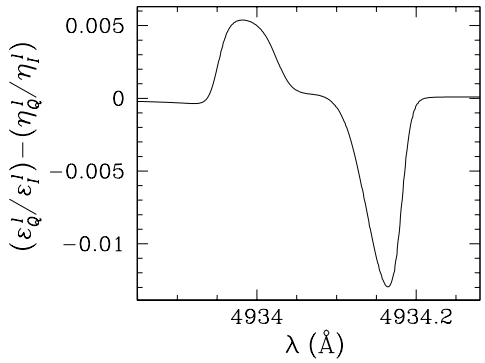


Fig. 18.— Theoretical $Q/I$ profile of the Ba II $D_1$ line calculated according to equation 13, in the absence of magnetic fields and without any contribution of the continuum. For the Doppler width, the anisotropy factor, and the average number of photons have been used the same values of § 4.8.

field geometries considered in this work.

Figure 18 shows the ratio $(\varepsilon_Q^l/\varepsilon_I^l)-(\eta_Q^l/\eta_I^l)$ for the $D_1$ line in the absence of magnetic fields. As expected, since the atomic polarization is quite similar in the upper and lower levels of the $D_1$, dichroism is much more important in this line, and the profiles obtained through equations (14) and (13) are quite different from each other. However, even taking into account dichroism, we are not able to reproduce the observed profile.

## B. ANALYTICAL RESULTS FOR A TWO-LEVEL ATOM APPLIED TO THE Ba II D LINES

In this work we have described the Ba II ion through a three level model atom that allowed us to study both the $D_1$ and $D_2$ lines; we have taken into account the ground level polarization, the stimulated emission effects and, finally, the effects of a magnetic field. At this level a numerical approach of the problem is absolutely necessary. However, as described in detail in § 10 of LL04, by introducing some simplifying approximations it is possible to obtain analytical expressions for the atomic density-matrix elements and, through these, for the radiation transfer coefficients of the atomic system. These analytical expressions are very useful in order to understand the physics of the phenomenon under investigation, which could remain quite hidden within a numerical approach. The basic approximation is to consider a two-level atom. The only difference between our three-level model atom and a two-level atom lies in the fact that in the SEEs of our model the ground level feels the effect of both transitions towards the two upper levels considered. However, the numerical solution of the SEEs showed that the upper level of the $D_2$ line is much more polarized than the ground

level, so that, as far as the $D_2$ line is considered, the polarization of the ground level, as a first approximation, can be neglected and our atomic system can be treated as a two-level atom. We can therefore apply the equations of § 10 of LL04 to calculate the upper level density-matrix elements or the emission coefficients of the various Ba II isotopes, described as two-level atoms with HFS, and two-level atoms without HFS, with unpolarized lower level. Neglecting the stimulated emission effects (which is a good approximation whenever the incident radiation field, as in our case, is weak), and in the absence of the magnetic field, the emission coefficient of a two-level atom without HFS is (see eq.[10.16] of LL04)

$$\begin{aligned} \varepsilon_i(\nu,\mathbf{\Omega}) &= \frac{h\nu}{4\pi}\mathcal{N}_\ell B(\alpha_\ell J_\ell \rightarrow \alpha_u J_u)\phi(\nu_0-\nu) \\ &\quad \times \sum_{KQ} W_K(J_\ell,J_u)(-1)^Q \mathcal{T}^K_Q(i,\mathbf{\Omega}) J^K_{-Q}(\nu_0) \ , \end{aligned} \tag{B1}$$

where $\mathcal{N}_\ell$ is the number density of atoms in the ground level[16], and where

$$W_K(J_\ell,J_u) = 3(2J_u+1)\left\{ \begin{array}{ccc} 1 & 1 & K \\ J_u & J_u & J_\ell \end{array} \right\}^2 \ . \tag{B2}$$

For 90° scattering of a radiation field with cylindrical symmetry around the direction of propagation (as in our case), from equation (B1) we obtain

$$p_Q \equiv \frac{\varepsilon_Q}{\varepsilon_I} = \frac{3W_2(1/2,3/2)}{4/w - W_2(1/2,3/2)} \ . \tag{B3}$$

This expression shows that for the isotopes without HFS the fractional polarization $p_Q$ does not depend on frequency, as found in § 4.1 (Fig. 5). Substituting the numerical values of the various quantities ($w = 0.037$ and $W_2(1/2,3/2) = 0.5$) we obtain the value of 1.4%, as found with numerical calculations. The expression of the emission coefficient of a two-level atom with HFS (eq. [10.166] of LL04) is much more complicated and will not be written here. Anyway, as shown in § 10.22 of LL04, at frequencies very distant from the 'center of gravity', the multiplet behaves in resonance scattering as a simple transition between two levels without HFS. The fractional polarization, therefore, at these frequencies is still described by equation (B3). This result justifies the fact that at large distances from the line center the fractional polarization of the isotopes with HFS reaches the same value as the isotopes without HFS. It is important to stress that this asymptotic behaviour of the isotopes with HFS is strongly dependent on the interferences between the various HFS magnetic sublevels of the

[16]Note that for a two level atom $\mathcal{N} = \mathcal{N}_\ell + \mathcal{N}_u$ while, for our model atom, $\mathcal{N} = \mathcal{N}_\ell + \mathcal{N}_u^{D_2} + \mathcal{N}_u^{D_1}$. As far as lower level polarization is neglected, this is the only difference between a two-level atom and our model atom.

$D_2$ upper level. Because of the small frequency distance between the various components of the HFS multiplet with respect to their natural width, the analytical expression of the emission coefficients of the isotopes with HFS cannot be simplified in the neighbourhood of the various transitions. Nevertheless, we can qualitatively justify the decrease of the fractional polarization at the wavelength positions of the various components of the HFS multiplet by considering the frequency integrated emission coefficients of the isotopes with HFS

$$\begin{aligned}\tilde{\varepsilon}_i(\mathbf{\Omega}) &= \int_{\Delta\nu} \varepsilon_i(\nu,\mathbf{\Omega})\mathrm{d}\nu \\ &= \frac{h\nu}{4\pi}\mathcal{N}_\ell\, B(\alpha_\ell J_\ell \rightarrow \alpha_u J_u) \sum_{KQ} [W_K(\alpha_\ell J_\ell I, \alpha_u J_u)]_{\rm hfs}\,(-1)^Q\,\mathcal{T}^K_Q(i,\mathbf{\Omega}) J^K_{-Q}(\nu_0) \quad \text{(B4)}\end{aligned}$$

where the interval $\Delta\nu$ is sufficiently broad to fully cover all the Zeeman components of the line, and where

$$[W_K(\alpha_\ell J_\ell I, \alpha_u J_u)]_{\rm hfs} = W_K(J_\ell, J_u)[D_K(\alpha_u J_u I)]_{\rm hfs} \quad . \quad \text{(B5)}$$

The quantity $[D_K(\alpha_u J_u I)]_{\rm hfs}$ is the depolarizing factor due to HFS and it is given by

$$\begin{aligned}[D_K(\alpha J I)]_{\rm hfs} &= \frac{1}{(2I+1)}\sum_{FF'}(2F+1)(2F'+1)\left\{ \begin{array}{ccc} J & J & K \\ F & F' & I \end{array} \right\}^2 \\ &\times \frac{1}{1+2\pi \mathrm{i}\nu_{\alpha JIF',\alpha JIF}/A(\alpha J \rightarrow \alpha_\ell J_\ell)} \quad . \quad \text{(B6)}\end{aligned}$$

For the isotope 137 the depolarizing factor $[D_2(J{=}3/2, I{=}3/2)]_{\rm hfs}$ is equal to 0.27, and the frequency integrated fractional polarization, that in complete analogy with equation (B3) has the form

$$\tilde{p}_Q \equiv \frac{\tilde{\varepsilon}_Q}{\tilde{\varepsilon}_I} = \frac{3W_2(J_\ell, J_u)[D_K(\alpha_u J_u I)]_{hfs}}{4/w - W_2(J_\ell, J_u)[D_K(\alpha_u J_u I)]_{hfs}} \quad , \quad \text{(B7)}$$

is equal to 0.0038. Comparing this value with 0.014, the value of $p_Q$ previously found for the isotopes without HFS (note that for these isotopes $p_Q$ is equal to $\tilde{p}_Q$), we can clearly see the depolarizing effect of the HFS.

For the $D_1$ line the quantity $W_2(1/2, 1/2)$ is zero and, taking into account equations (B1) and (B7), it is easy to see that the Stokes $Q$ emission coefficient of the isotopes without HFS has to be constant and equal to zero, while the frequency integrated Stokes $Q$ emission coefficient of the isotopes with HFS has to be zero, as found with numerical calculations in § 4.8. However, as previously said, for the case of the $D_1$ line the approximation of unpolarized lower level is not good anymore. Some analytical results that it is possible to obtain taking into account the polarization of the lower level are derived in LL04.

In the presence of a vertical magnetic field equation (B7) generalizes into

$$\tilde{p}_Q \equiv \frac{\tilde{\varepsilon}_Q}{\tilde{\varepsilon}_I} = \frac{3[W_{220}(\alpha_\ell J_\ell I \alpha_u J_u; B)]_{\rm hfs}}{4/w - [W_{220}(\alpha_\ell J_\ell I \alpha_u J_u; B)]_{\rm hfs}} \quad , \quad \text{(B8)}$$

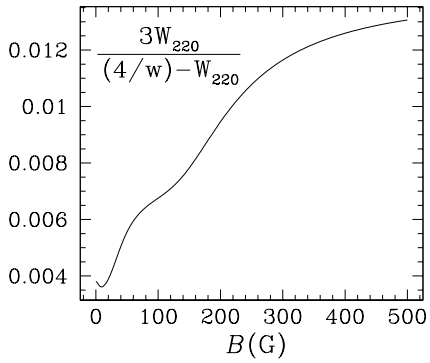


Fig. 19.— Frequency integrated fractional polarization for the isotope 137 in a 90° scattering event in the presence of a vertical magnetic field, as function of the magnetic field strength. Calculations refer to the Ba II $D_2$ line.

where the general expression of the quantity $[W_{KK'Q}(\alpha_\ell J_\ell I \alpha_u J_u; B)]_{\rm hfs}$ is given in LL04 (eq. [10.167]). Figure 19 shows that there is an increase of $\tilde{p}_Q$ for vertical magnetic fields ranging between 0 and 500 G (see Fig. 7).

## C. AVERAGE OF THE EMISSION COEFFICIENTS OVER THE MAGNETIC FIELD DIRECTIONS

The only quantity that depends on the magnetic field orientation in the general expression of the emission coefficients (§ 2.1, eq. [6]) is the product

$$\left[\mathcal{T}^K_Q(j,\mathbf{\Omega})\right]_B \left[{}^{\alpha_u J_u I}\rho^{K_u}_{Q_u}(F'_u, F''_u)\right]_B \ , \tag{C1}$$

where the label $B$ means that the quantity is calculated in the magnetic field reference system. We already observed (§ 3) that the spherical statistical tensors calculated in the magnetic reference system, because of the symmetry of the problem, do not depend on the azimuth of the magnetic field, $\chi_B$, but only on its inclination with respect to the local vertical, $\theta_B$. For this reason all the dependence on $\chi_B$ is included into the geometrical tensor $[\mathcal{T}^K_Q(j,\mathbf{\Omega})]_B$. The expression of the tensor $\mathcal{T}^K_Q$ in terms of rotation matrices is given by (eq. [5.159] of LL04)

$$\left[\mathcal{T}^K_Q(j,\mathbf{\Omega})\right]_B = \sum_P t^K_P(j) \mathcal{D}^K_{PQ}(R_0) \ , \tag{C2}$$

where $\mathcal{D}$ is the rotation matrix, $R_0$ is the rotation bringing the reference system $(\mathbf{e}_a(\mathbf{\Omega}), \mathbf{e}_b(\mathbf{\Omega}), \mathbf{\Omega})$, with $\mathbf{e}_a(\mathbf{\Omega})$ the reference direction, into the reference system with the $z$ axis directed along

the magnetic field, and where $t_P^K(j)$ is a scalar quantity that does not depend on the particular geometry of the problem (cf. eq. [5.160] of LL04). The relation between the geometrical tensor $\mathcal{T}_Q^K$ calculated in the magnetic field reference system, and the same quantity calculated in the local vertical reference system (with the $z$ axis directed along the local vertical) is

$$\left[\mathcal{T}_Q^K(j,\mathbf{\Omega})\right]_B = \sum_A \left[\mathcal{T}_A^K(j,\mathbf{\Omega})\right]_V \mathcal{D}_{AQ}^K(R_1) \ , \tag{C3}$$

where the label $V$ means that the corresponding quantity is calculated into the local vertical reference system, and where $R_1$ is the rotation bringing the local vertical reference system into the magnetic field reference system. In the geometry of our problem the rotation $R_1$ is defined by the Euler angles $(\chi_B, \theta_B, 0)$. Obviously, because of its definition, $[\mathcal{T}_A^K(j,\mathbf{\Omega})]_V$ does not depend on the magnetic field orientation: in analogy with equation (C2) we can write

$$\left[\mathcal{T}_A^K(j,\mathbf{\Omega})\right]_V = \sum_P t_P^K(j) \mathcal{D}_{PA}^K(R_2) \ , \tag{C4}$$

where $R_2$ is the rotation that brings the reference system $(\mathbf{e}_a(\mathbf{\Omega}), \mathbf{e}_b(\mathbf{\Omega}), \mathbf{\Omega})$ into the local vertical reference system. Substituting equation (C3) into the expression (C1) we obtain

$$\left[\mathcal{T}_Q^K(j,\mathbf{\Omega})\right]_B \left[{}^{\alpha_u J_u I}\rho_{Q_u}^{K_u}(F'_u, F''_u)\right]_B = \sum_A \left[\mathcal{T}_A^K(j,\mathbf{\Omega})\right]_V \mathcal{D}_{AQ}^K(R_1) \left[{}^{\alpha_u J_u I}\rho_{Q_u}^{K_u}(F'_u, F''_u)\right]_B \ , \tag{C5}$$

where we see that all the dependence on $\chi_B$ is included in the rotation matrix $\mathcal{D}_{AQ}^K(R_1)$. Recalling the expression of the rotation matrices in terms of the reduced rotation matrices (cf. eq. [2.68] of LL04), and recalling the Euler angles corresponding to the rotation $R_1$, we have

$$\mathcal{D}_{AQ}^K(R_1) = \mathrm{e}^{-\mathrm{i}A\chi_B} d_{AQ}^K(\theta_B) \ , \tag{C6}$$

where $d_{AQ}^K$ is the reduced rotation matrix, which depends only on the second Euler angle of the rotation, in our case the inclination of the magnetic field. Averaging on $\chi_B$ reduces therefore to calculate the integral

$$\frac{1}{2\pi} \int_0^{2\pi} \mathrm{e}^{-\mathrm{i}A\chi_B} \mathrm{d}\chi_B \ . \tag{C7}$$

It is easy to see that the integral is different from zero only if $A = 0$, and that, in this case, it is equal to 1. Averaging the emission coefficients over $\chi_B$, the magnetic field azimuth, is therefore equivalent to substitute expression (C1) with

$$\left[\mathcal{T}_0^K(j,\mathbf{\Omega})\right]_V d_{0Q}^K(\theta_B) \left[{}^{\alpha_u J_u I}\rho_{Q_u}^{K_u}(F'_u, F''_u)\right]_B \ . \tag{C8}$$

Now all the quantities depend only on the magnetic field inclination, and we can complete numerically (for example by a Gaussian quadrature) the average over the magnetic field orientation.

## REFERENCES

Becker, W., Blatt, R., & Werth, G. 1981, J. Physique Coll., 42, C8-339

Bommier, V. 1980, A&A, 87, 109

Casini, R., Landi Degl'Innocenti, E., Landolfi, M., & Trujillo Bueno, J. 2002, ApJ, 573, 864

Landi Degl'Innocenti, E., & Landolfi, M. 2004, Polarization in Spectral Lines (Dordrecht: Kluwer)

Kopfermann, H. 1958, Nuclear Moments (New York: Academic Press)

Moore, C. E. 1958, Atomic Energy Levels: as derived from the analyses of optical spectra, Vol.III (Washington National Bureau of Standards)

Pierce, K. 2000, in Allen's Astrophysical Quantities, ed. A. N. Cox (4th ed.; New York: Springer), 355

Stenflo, J. O. 1997, A&A, 324, 344

Stenflo, J. O., & Keller, C. U. 1997, A&A, 321, 927

Stenflo, J. O., Keller, C. U., & Gandorfer, A. 1998, A&A, 329, 319

Stenflo, J. O., Keller, C. U., & Gandorfer, A. 2000, A&A, 335, 789

Stenflo, J. O., Gandorfer, A., Holzreuter, R., Gisler, D., Keller, C. U., & Bianda, M. 2002, A&A, 389, 314

Stenflo, J.O. 2003, in ASP Conf. Ser. 307, Solar Polarization 3, ed. J. Trujillo Bueno, & J. Sánchez Almeida (San Francisco: ASP), 385

Trujillo Bueno, J. 2003, in ASP Conf. Ser. 307, Solar Polarization 3, ed. J. Trujillo Bueno, & J. Sánchez Almeida (San Francisco: ASP), 407

Trujillo Bueno, J., Casini, R., Landolfi, M., & Landi Degl'Innocenti, E. 2002, ApJ, 566, L53

Villemoes, P., Arnesen, A., Heijkenskjöld, F., & Wännström, A. 1993, J. Phys. B, 26, 4289

Wendt, K., Ahmad, S. A., Buchinger, F., Mueller, A. C., Neugart, R., & Otten, E. W. 1984, Z. Phys. A, 318, 125

Wendt, K., Ahmad, S. A., Ekström, C., Klempt, W., Neugart, R., & Otten, E. W. 1988, Z. Phys. A, 329, 407